UNCLASSIFIED

AD **274 612**

Reproduced
by the

ARMED SERVICES TECHNICAL INFORMATION AGENCY
ARLINGTON HALL STATION
ARLINGTON 12, VIRGINIA

UNCLASSIFIED

AFOSR-TN-62-2232

R. J. SWIGART

A THEORY OF ASYMMETRIC HYPERSONIC BLUNT-BODY FLOWS

JANUARY
1962

SUDAER
NO. 120

Department of Aeronautics & Astronautics
Stanford University
Stanford, California

A THEORY OF ASYMMETRIC HYPERSONIC BLUNT-BODY FLOWS

by

Rudolph J. Swigart

SUDAER No. 120

January 1962

ABSTRACT

The problem of supersonic and hypersonic flow past blunt bodies at small angles of attack is considered. Two-dimensional asymmetric as well as three-dimensional flow is analyzed.

The method of analysis is an inverse one, that is, the shock-wave shape and free stream conditions are known, and the corresponding body shape and flow field are to be determined. A semi-analytical, semi-numerical solution to the full inviscid equations of motion is obtained by expanding the stream function and density in double McLaurin series in powers of distance from the shock-wave axis of symmetry and powers of the shock-wave angle of attack. These expansions bring about a separation of variables that reduces the problem to numerical integration of ordinary differential equations for the power-series coefficients. The integration can be accomplished only by truncating the series. This truncation may be performed after keeping any desired number of terms in the series about the shock symmetry-axis. Only first-order terms in shock-wave angle of attack are retained.

Solutions at zero angle of attack are obtained as a special case of the general problem. Results at zero angle are obtained for shock waves that are portions of circles, parabolas, spheres, and paraboloids of revolution at a free stream Mach number, M, of infinity and ratio of specific heats, γ, of 1.4. The first three truncations are carried out for the parabolic and spherical shock, whereas the first four truncations are calculated for the circular and paraboloidal shock. In all cases the stagnation-point density is obtained to five-significant-figure accuracy in two truncations. Standoff distance is obtained to four-place accuracy in three truncations. Convergence away from the axis of symmetry is not so rapid. Body shapes out to the sonic point converge in three truncations for the two-dimensional cases. However, axisymmetric body shapes and both two-dimensional and axisymmetric sonic line positions and surface pressure distributions out to the sonic point are not converged in four truncations, but are very close to being so.

Comparison with results obtained using Van Dyke's and Garabedian's numerical solutions indicates that the method under consideration is more accurate than the Van Dyke method.

The first three truncations are calculated for parabolic and paraboloidal shock waves at small angle of attack and infinite free stream Mach number. The specific-heat ratio, γ, takes on the values 1.4, 1.2, 1.1, and 1.05. For all cases, the streamline that wets the body passes through the shock wave slightly above the point where the shock wave is normal, and consequently does not possess maximum entropy. Although these results provide a counter example to the conjecture that any isolated convex body in a supersonic stream is wetted by the streamline of maximum entropy, the stagnation and maximum-entropy streamlines are very close to each other, thus suggesting that the conjecture may be a good practical approximation. Indications are that, in the Newtonian limit ($M = \infty$, $\gamma = 1$), the conjecture is true for the shock shapes considered.

A symmetrical shock wave at angle of attack is produced by a body that is asymmetric to the shock axis of symmetry. However, a conic section may be fitted to the converged body shape out to the sonic point. This is done for the third-truncation body that produces a parabolic shock at angle of attack of 10°. The body is closely approximated by a prolate ellipse at angle of attack of 14.2°. Thus, for the two-dimensional case, the shock wave is seen to rotate more slowly than the body as angle of attack is imposed. The same result is true for the third-truncation body in the three-dimensional case.

TABLE OF CONTENTS

LIST OF FIGURES

ACKNOWLEDGMENT

I. INTRODUCTION

For more than a decade, theoreticians interested in high-speed gasdynamics have been seeking a solution to the problem of supersonic and hypersonic flow past a blunt body that combines the advantages of minimum computational difficulty with maximum accuracy of results. Physically, the problem under consideration is the following. A blunt-nosed configuration is traveling through a uniform gas at a flight Mach number greater than unity. A detached shock wave forms ahead of the body at a position depending on the body shape, flight direction and Mach number, and certain physical properties of the gas. The gas ahead of the shock wave is unaffected by the presence of the body. It is desired to determine the flow properties (e.g., velocity, pressure, density) in the region between the shock and the body. In general, this region may be divided into two subregions, depending on the magnitude of the local flow Mach number with respect to unity. The locus of points at which the local flow Mach number is unity is called the sonic line. If one considers steady flow relative to the body and denotes by M and M_ℓ the free stream and local Mach numbers respectively, then an example of the above situation is here depicted.
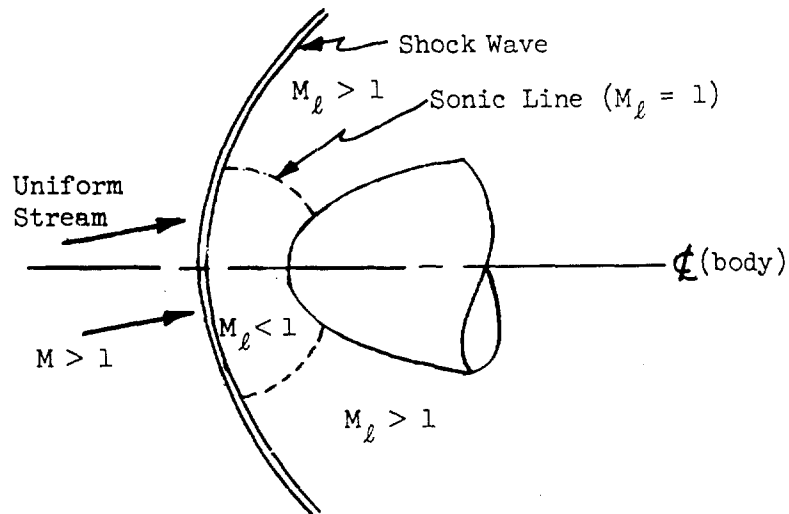
Mathematically, the problem considered is governed by highly non-linear differential equations in a domain possessing a free boundary along which initial values may be determined if the boundary shape and free stream conditions are known. The governing equations are of elliptic type in the subsonic region ($M_\ell < 1$) and of hyperbolic type in the supersonic region ($M_\ell > 1$). The initial-value problem for hyperbolic equations is well posed and yields to solution using the well-known theory of characteristics. The initial-value problem for elliptic equations is, however, poorly posed, and much of the effort expended on the blunt-body problem has been confined to its solution in the subsonic region. Attempts have been made to solve the problem by both inverse and direct methods. In the inverse method, the shape of the detached shock and the free stream conditions are prescribed, and the corresponding body shape and flow field are to be determined. In the direct method, the body shape and free stream conditions are pre-scribed, and the corresponding shock wave shape and flow field are to be determined. References [1] and [2] contain detailed reviews of and extensive references to previous work for plane-symmetric and axi-symmetric shapes at zero angle of attack, i.e., bodies whose flight direction is parallel to the body axis of symmetry.

The methods now in popular use for solving the zero-angle problem in the entire subsonic region to a high degree of accuracy are numerical in nature and require the use of high-speed electronic computing machines. Two such methods are Van Dyke's [3] approach to the inverse problem and Belotserkovskii's [4] solution to the direct problem. Van Dyke's analysis essentially reduces the solution of the conservation equations for steady, inviscid flow of a perfect, non-heat-conducting gas to numerical integration of two coupled partial differential equations for the density and stream function. Belotserkovskii, on the other hand, by assuming a polynomial variation between the shock and body for certain flow quantities, reduces the problem to integration of ordinary differ-ential equations. Practical experience has shown that both of these methods require a large amount of skill on the part of the numerical analyst in order to obtain satisfactory solutions for other than simple

- 2 -

body shapes such as spheres or circular cylinders. Hence, even though these methods yield fairly high accuracy, they possess a moderate amount of computational difficulty.

In contrast to the zero-angle problem, comparatively little effort has been expended on the problem of the blunt body at angle of attack in either the two-dimensional or three-dimensional cases. Both Mangler [5] and Vaglio-Laurin and Ferri [6] suggest computational methods for attacking such problems, but neither presents results using the analyses proposed. They both obtain solutions to the zero-angle inverse problem by introducing the stream function as an independent variable through a von Mises transformation. The resulting partial differential equations are then numerically integrated from the shock to the body using a marching technique. Mangler suggests an extension of this marching technique to the three-dimensional angle-of-attack problem formulated in terms of a pair of stream functions. The approach of Vaglio-Laurin and Ferri to the problem of the blunt body at incidence involves a first-order perturbation of the flow variables about their zero-angle values.

Vaglio-Laurin [7] has developed another approach to the blunt-body problem at zero or finite incidence which involves the successive refinement of an approximate solution by application of the PLK method. Results for configurations at both zero and finite angle of attack using the analysis are presented in ref.[7].

The success, however, of Mangler's and Vaglio-Laurin's methods for the solution of the angle-of-attack problem depends on an assumption regarding a basic property of asymmetric supersonic flows. The assumption is that the body is covered by the streamline that crosses the shock at right angles and thus possesses maximum entropy. Mangler has conjectured that such a condition might be a feature of any flow, whereas Vaglio-Laurin [7, p.19] purportedly has proven this to be true for two-dimensional asymmetric configurations. However, the proof has been found to be faulty, and Vaglio-Laurin is in accord with this conclusion (private communication).

The analysis that follows yields solutions for two-and three-dimensional supersonic and hypersonic flow past blunt bodies at small angles of incidence. The method is an inverse one, that is, the shock-wave shape, free stream conditions, and angle of incidence of the shock wave are known, and the corresponding body and flow field are to be obtained. The equations of motion are solved using a semi-analytical, semi-numerical approach which reduces the problem to numerical integration of ordinary differential equations. The solution may be carried to any desired degree of accuracy and requires no extensive numerical analytical skill. Moreover, no assumption need be made regarding the behavior of the maximum-entropy streamline. Its position in the flow is obtained as part of the solution. Results at zero incidence are obtained as a special case of the general problem. Although the examples chosen are for specific shock shapes at infinite Mach number and, in the majority of cases, a specific-heat ratio of 1.4, the analysis is performed for the general case. The method of extension to higher angles is obvious and introduces no new difficulties.

II. ANALYSIS

A. Coordinate System

The coordinate system adopted is that developed by Van Dyke [3].
The detached shock wave is described by a conic section so that it is
a portion of a hyperboloid of revolution, paraboloid, prolate ellipsoid,
sphere, or oblate ellipsoid. In cylindrical polar coordinates originat-
ing from its vertex (Fig. 1), any such shock has the equation

$$r^2 = 2R_s x - Bx^2 \tag{1}$$

where R_s is the nose radius of the shock and B is a parameter char-
acterizing the eccentricity of the conic section. B is negative for
hyperboloids, zero for paraboloids, positive for ellipsoids, and unity
for a sphere.

An orthogonal coordinate system (ξ, η) that contains the shock
wave as a coordinate surface is defined by

$$\frac{x}{R_s} = \frac{1}{B}\left[1 - \sqrt{(1 - B\xi^2)(1 - B + B\eta^2)} \right] \tag{2a}$$

$$\frac{r}{R_s} = \xi\eta \tag{2b}$$

Special cases are

$$\frac{x}{R_s} = \tfrac{1}{2}(1 + \xi^2 - \eta^2) \qquad \text{for the parabola} \quad (B = 0) \tag{2c}$$

$$\frac{x}{R_s} = 1 - \eta\sqrt{1 - \xi^2} \qquad \text{for the circle} \quad (B = 1) \tag{2d}$$

The shock wave is described by $\eta = 1$.

In this coordinate system, with the azimuthal angle φ as the
third orthogonal coordinate, the differential line element ds is given

- 5 -

by

$$ds^2 = h_1^2\,d\xi^2 + h_2^2\,d\eta^2 + h_3^2\,d\varphi^2$$

$$\equiv \left(\frac{C\xi^2 + \eta^2}{1 - B\xi^2}\,d\xi^2 + \frac{C\xi^2 + \eta^2}{C + B\eta^2}\,d\eta^2 + \nu\xi^2\eta^2\,d\varphi^2 \right) R_s^2 \qquad (3)$$

where $C \equiv 1 - B$. Here ν is a geometric parameter, being 0 for plane and 1 for axisymmetric or three-dimensional flow.

B. Differential Equations, Initial Conditions, and Method of Solution

Denote by $\vec{q}, \rho,$ and p the velocity, density, and pressure non-dimensionalized with respect to the free stream speed q_∞, the free stream density ρ_∞, and twice the free stream dynamic pressure $\rho_\infty q_\infty^2$, respectively. Then, the equations expressing conservation of mass, momentum, and entropy for steady inviscid flow of a perfect, non-heat-conducting gas having constant specific heats are

$$\nabla \cdot (\rho\vec{q}) = 0 \qquad (4a)$$

$$\rho\vec{q}\cdot\nabla\vec{q} + \nabla p = 0 \qquad (4b)$$

$$\vec{q}\cdot\nabla(p/\rho^\gamma) = 0 \qquad (4c)$$

where γ is the adiabatic exponent.

We set $R_s = 1$ without loss of generality. Eqs. (4a), (4b) and (4c) become, in (ξ, η, φ) coordinates

$$\left[(\xi\eta)^\nu \sqrt{\frac{C\xi^2 + \eta^2}{C + B\eta^2}}\,\rho u \right]_\xi + \left[(\xi\eta)^\nu \sqrt{\frac{C\xi^2 + \eta^2}{1 - B\xi^2}}\,\rho v \right]_\eta$$

$$+ \left[\frac{C\xi^2 + \eta^2}{\sqrt{(1 - B\xi^2)(C + B\eta^2)}}\,\rho w \right]_\varphi = 0 \qquad (5a)$$

$$\rho \left[uu_\xi - \frac{C\xi v^2}{C\xi^2 + \eta^2} + \sqrt{\frac{C + B\eta^2}{1 - B\xi^2}}\, v \left(u_\eta + \frac{\eta u}{C\xi^2 + \eta^2} \right) \right.$$

$$\left. + \frac{w}{\xi\eta} \sqrt{\frac{C\xi^2 + \eta^2}{1 - B\xi^2}}\, u_\varphi - \frac{w^2}{\xi} \right] + p_\xi = 0 \qquad (5b)$$

$$\rho \left[vv_\eta - \frac{\eta u^2}{C\xi^2 + \eta^2} + \sqrt{\frac{1 - B\xi^2}{C + B\eta^2}}\, u \left(v_\xi + \frac{C\xi v}{C\xi^2 + \eta^2} \right) \right.$$

$$\left. + \frac{w}{\xi\eta} \sqrt{\frac{C\xi^2 + \eta^2}{C + B\eta^2}}\, v_\varphi - \frac{w^2}{\eta} \right] + p_\eta = 0 \qquad (5c)$$

$$\rho \left[ww_\varphi + u\eta \sqrt{\frac{1 - B\xi^2}{C\xi^2 + \eta^2}}\, (w + \xi w_\xi) + v\xi \sqrt{\frac{C + B\eta^2}{C\xi^2 + \eta^2}}\, (w + \eta w_\eta) \right] + p_\varphi = 0$$

$$(5d)$$

$$u \sqrt{\frac{1 - B\xi^2}{C\xi^2 + \eta^2}}\, (p/\rho^\gamma)_\xi + v \sqrt{\frac{C + B\eta^2}{C\xi^2 + \eta^2}}\, (p/\rho^\gamma)_\eta + \frac{w}{\xi\eta}\, (p/\rho^\gamma)_\varphi = 0 \quad (5e)$$

Here u, v, and w are the components of $\vec{q}$ in the ξ, η, and φ directions, and subscripts ξ, η, and φ denote partial differentiation in the usual sense.

Since the method of solution varies slightly between the two-and three-dimensional cases, departure will now be taken from a concurrent treatment.

1. Plane Flow

Equations (5a) - (5e) apply with $v = w = \frac{\partial}{\partial \varphi} = 0$. The first (continuity) equation is satisfied by introducing a stream function defined by

$$\psi_\eta = \sqrt{\frac{C\xi^2 + \eta^2}{C + B\eta^2}}\, \rho u \quad ; \quad \psi_\xi = -\sqrt{\frac{C\xi^2 + \eta^2}{1 - B\xi^2}}\, \rho v \tag{6}$$

then the last (entropy) equation simply states that

$$p = \rho^\gamma f(\psi) \tag{7}$$

where the functional form of f is determined by the boundary conditions at the shock. Using equation (7) to eliminate the pressure from the equations of motion yields

$$\left[\gamma \frac{C\xi^2 + \eta^2}{1 - B\xi^2}\, f\rho^{\gamma+1} - \psi_\xi^2 \right] \frac{\rho_\eta}{\rho} = \psi_\eta \psi_{\xi\xi} + \frac{\eta}{C\xi^2 + \eta^2}\left(\psi_\xi^2 + \frac{C + B\eta^2}{1 - B\xi^2}\, \psi_\eta^2 \right) \tag{8a}$$

$$- \psi_\xi \psi_{\xi\eta} - \psi_\xi \psi_\eta \frac{\rho_\xi}{\rho} - \frac{B\xi}{1 - B\xi^2}\, \psi_\xi \psi_\eta - \frac{C\xi^2 + \eta^2}{1 - B\xi^2}\, \rho^{\gamma+1}\, f'\psi_\eta$$

$$\psi_\xi \psi_{\eta\eta} = \psi_\eta \psi_{\xi\eta} + \psi_\eta\left(\psi_\xi \frac{\rho_\eta}{\rho} - \psi_\eta \frac{\rho_\xi}{\rho} \right) - \frac{C\xi}{C\xi^2 + \eta^2}\left(\frac{1 - B\xi^2}{C + B\eta^2}\, \psi_\xi^2 + \psi_\eta^2 \right) \tag{8b}$$

$$- \frac{B\eta}{C + B\eta^2}\, \psi_\xi \psi_\eta + \frac{C\xi^2 + \eta^2}{C + B\eta^2}\, f\rho^{\gamma+1}\left(\gamma \frac{\rho_\xi}{\rho} + \frac{f'}{f}\, \psi_\xi \right)$$

Thus far, the attitude of the body with respect to the free stream, or, since we are considering the inverse problem, the angle of the uniform free stream with the shock axis of symmetry, has not entered into the mathematical formulation. The angle of attack of the shock will, however, appear in the boundary conditions and in the explicit expression for $f(\psi)$. These conditions will be derived by employing McLaurin series expansions about zero angle of attack and retaining first-order terms in shock angle of attack, ϵ. Setting ϵ equal to zero recovers the zero-angle conditions.

Moreover, in the angle-of-attack problem, the position in the flow ahead of the shock wave of the streamline that wets the body is not known a priori, but must be obtained as part of the solution. A fundamental question in the analysis of hypersonic flows past inclined blunt bodies concerns the behavior of this streamline. It has been conjectured [5,7] that any isolated convex body in a uniform supersonic stream is covered by the fluid of maximum entropy in the flow. This means that the stagnation streamline must have crossed the bow shock where it is a normal shock wave. To determine the position of the stagnation stream-line in the free stream and thus possibly disprove the conjecture, the formulation of the angle-of-attack problem requires the introduction of an additional parameter, δ (Fig. 2). The quantity $c\delta$ is a measure of the distance of the body streamline in the free stream from a given reference line. This reference line is at angle ϵ to the x-axis and, in general, is taken to pass through the point $\frac{x}{R_s} = \frac{1}{B}$, $\frac{r}{R_s} = 0$. However, in the singular case of the parabola ($B = 0$), the reference line is taken through the focus of the parabola ($\frac{x}{R_s} = \frac{1}{2}$, $\frac{r}{R_s} = 0$).

Values of u, v, p, ρ just behind the shock wave ($\eta = 1$) are found from the oblique shock relations (e.g., ref. [8]) in terms of the angle that the tangent to the bow wave makes with the free stream direction. Expressing this angle in terms of the slope of the bow wave, $\frac{\sqrt{1 - B\xi^2}}{B}$, and ϵ, using eqs.(6), and retaining first order terms in ϵ, results in the initial conditions

$$\rho = \frac{(\gamma + 1)M^2(1 - B\xi^2 - 2\epsilon\xi\sqrt{1 - B\xi^2})}{(\gamma - 1)M^2(1 - B\xi^2 - 2\epsilon\xi\sqrt{1 - B\xi^2}) + 2(1 + C\xi^2)}$$

$$\tag{9a}$$

$$\psi = \xi + \epsilon\left(\frac{\sqrt{1 - B\xi^2}}{B} + \delta\right) \quad ; \quad \psi_\eta = \rho(\xi + \epsilon\sqrt{1 - B\xi^2})$$

$$\text{at} \quad \eta = 1$$

and gives for the function $f(\psi)$

$$f(\psi) = \frac{2\gamma M^2(1 - B\psi^2 + 2\epsilon B\psi\delta) - (\gamma - 1)\left[1 + C\psi^2 - 2\epsilon C\psi\left(\frac{\sqrt{1 - B\psi^2}}{B} + \delta\right)\right]}{\gamma(\gamma + 1)M^2\left\{1 + C\left[\psi^2 - 2\epsilon\psi\left(\frac{\sqrt{1 - B\psi^2}}{B} + \delta\right)\right]\right\}}$$

$$\times\left\{\frac{(\gamma-1)M^2(1-B\psi^2 + 2\epsilon B\psi\delta) + 2\left[1+C\psi^2 - 2\epsilon C\psi\left(\frac{\sqrt{1 - B\psi^2}}{B} + \delta\right)\right]}{(\gamma+1)M^2(1-B\psi^2 + 2\epsilon\psi B\delta)}\right\}^\gamma \tag{10a}$$

where M is the free stream Mach number. For the singular case of a parabolic shock wave ($B = 0$, $C = 1$), the expressions for ρ, ψ, ψ_η at $\eta = 1$, and for f are

$$\rho = \frac{(\gamma + 1)M^2(1 - 2\epsilon\xi)}{(\gamma - 1)M^2(1 - 2\epsilon\xi) + 2(1 + C\xi^2)}$$

$$\psi = \xi + \epsilon(\delta + \tfrac{1}{2} - \xi^2/2) \quad ; \quad \psi_\eta = \rho(\xi + \epsilon) \quad \text{at} \quad \eta = 1$$

$$\tag{9b}$$

$$f = \frac{2\gamma M^2(1 - 2\epsilon\psi) - (\gamma - 1)[1 + \psi^2 - 2\epsilon\psi(\delta - \tfrac{1}{2} - \psi^2/2)]}{\gamma(\gamma + 1)M^2[1 + \psi^2 - 2\epsilon\psi(\delta + \tfrac{1}{2} - \psi^2/2)]}$$

$$\times \left\{ \frac{(\gamma - 1)M^2(1 - 2\epsilon\psi) + 2[1 + \psi^2 - 2\epsilon\psi(\delta + \tfrac{1}{2} - \psi^2/2)]}{(\gamma + 1)M^2(1 - 2\epsilon\psi)} \right\}^\gamma \quad (10b)$$

The boundary condition at the body is

$$\psi = 0 \quad \text{at} \quad \eta = \eta_b . \tag{11}$$

The method of solution essentially consists of separation of variables in equations (8) - (11) by expanding the dependent variables in double McLaurin series about the shock axis of symmetry, $\xi = 0$, and about $\epsilon = 0$. Only first order terms in ϵ are retained. This leads to ordinary differential equations with corresponding boundary conditions for unknown functions of η which can be solved only by truncating the series. The resulting equations are readily integrated by standard numerical methods. The above procedure will now be carried out.

Set

$$\psi = f_{00}(\eta)\xi + f_{01}(\eta)\xi^3 + f_{02}(\eta)\xi^5 + 0(\xi^7)$$

$$+ \epsilon[f_{10}(\eta) + f_{11}(\eta)\xi^2 + f_{12}(\eta)\xi^4 + 0(\xi^6)] + 0(\epsilon^2) \tag{12a}$$

$$\frac{\gamma - 1}{\gamma + 1} \rho = g_{00}(\eta) + g_{01}(\eta)\xi^2 + g_{02}(\eta)\xi^4 + 0(\xi^6)$$

$$+ \epsilon[g_{10}(\eta)\xi + g_{11}(\eta)\xi^3 + g_{12}(\eta)\xi^5 + 0(\xi^7)] + 0(\epsilon^2) \tag{12b}$$

The first subscript on the functions of η is 0 for the zero angle of attack portion of the solution and 1 for the angle of attack portion, and the second subscript indicates the position of the term in its respective series. The forms of these expansions are readily ascertained by consideration of the initial conditions.

Expansions (12a) and (12b) are substituted into the differential equations (8) and boundary conditions (9) - (11). Equating coefficients of like powers of ξ and ϵ results in successive problems for f_{00}, g_{00}, g_{01} ; f_{00}, g_{00}, f_{01}, g_{01}, g_{02} ; etc. Thus the zero-order problem for f_{00} and g_{00} involves two equations which also contain g_{01} , the first-order problem for f_{00}, g_{00}, f_{01}, g_{01} involves four equations which also contain g_{02} , and so forth. The same pattern occurs in the successive equations for the angle-of-attack functions. This "backward influence" of g_{0n+1} in the nth-order problem is due to the ellipticity of the differential equations in the subsonic region, and is a mathematical manifestation of the physical fact that disturbances are propagated in all directions in a subsonic flow. This mathematical behavior may be contrasted, for example, with that of the equations determining the coefficients of the Blasius-series solution to the parabolic equations governing the laminar boundary layer on a blunt body. Substitution of the Blasius series into the governing differential equation and equating coefficients of like powers results in equations for the series coefficients which involve only one coefficient or depend only on lower order coefficients, and hence may be solved successively.

We return to the problem under consideration. To solve the nth-order zero-angle problem for f_{00}, f_{01}, $\cdots$ f_{0n} and g_{00}, g_{01} $\cdots$ g_{0n} , some determination must be made of g_{0n+1} . The simplest thing to do is to truncate the series by setting g_{0n+1} identically equal to zero. The resulting equations may then be integrated.

It is found that the differential equations for f_{00} and g_{00} are nonlinear, whereas the equations for succeeding terms in the zero-angle series are linear. The equations for all the angle of attack functions are linear and contain coefficients that depend on the zero-angle solution.

- 12 -

Integration is terminated and the body shape determined by the boundary condition (11). For the angle-of-attack problem, this condition also determines δ .

To illustrate the procedure, the equations and boundary conditions for the first and second truncations for a parabolic shock wave at $M = \infty$ will be presented.

After inserting series (12a) and (12b) into equations (8a), (8b), (9b), and (10b), and equating coefficients of like powers of ξ and ϵ , the following differential equations and initial conditions are obtained. (Primes indicate differentiation with respect to η . The powers of ξ and ϵ from whose coefficients the equation results are indicated in front of each equation).

Differential Equations

a) Zero angle

$$\xi^0, \ \epsilon^0: \quad \left(\frac{2\gamma}{\gamma-1} \, \eta^2 \, g_{00}^{(\gamma+1)} - f_{00}^2 \right) \frac{g_{00}'}{g_{00}} = \frac{f_{00}^2}{\eta} - f_{00} \, f_{00}' \tag{13a}$$

$$\xi, \ \epsilon^0: \quad f_{00} f_{00}'' = f_{00}' \left(f_{00}' + f_{00} \frac{g_{00}'}{g_{00}} \right) - \frac{f_{00}^2}{\eta^2} + \frac{4\eta^2}{\gamma-1} \, g_{00}^{(\gamma+1)} \left(\frac{\gamma g_{01}}{g_{00}} - f_{00}^2 \right) \tag{14a}$$

$$\xi^2, \ \epsilon^0: \quad \left(\frac{2\gamma}{\gamma-1} \, \eta^2 g_{00}^{(\gamma+1)} - f_{00}^2 \right) \left(\frac{g_{01}'}{g_{00}} - \frac{g_{01} g_{00}'}{g_{00}^2} \right) = - \left\{ \frac{2\gamma}{\gamma-1} \, g_{00}^{(\gamma+1)} \left(\eta^2 \left[(\gamma+1) \frac{g_{01}}{f_{00}} \right. \right. \right.$$

$$\left. - f_{00}^2 \right] + 1 \right) - 6 f_{00} f_{01} \right\} \frac{g_{00}'}{g_{00}} + 6 f_{00}' f_{01} + \frac{1}{\eta} \left(6 f_{00} f_{01} + f_{00}'^2 - \frac{f_{00}^2}{\eta^2} \right)$$

$$- 3(f_{00} f_{01}' + f_{00}' f_{01}) - 2 f_{00} f_{00}' \frac{g_{01}}{g_{00}} + \frac{4\eta^2}{\gamma-1} \, g_{00}^{(\gamma+1)} \, f_{00} f_{00}' \tag{15a}$$

- 23 -

$$\xi^3, \epsilon^0: \quad f_{00}f_{01}'' = -3f_{01}f_{00}'' + f_{00}'\left[3f_{01}' + f_{00}\left(\frac{g_{01}'}{g_{00}} - \frac{g_{01}g_{00}'}{g_{00}^2}\right) + 3f_{01}\frac{g_{00}'}{g_{00}}\right.$$

$$\left. - 2f_{00}'\frac{g_{01}}{g_{00}}\right] + f_{01}'\left(f_{00}' + f_{00}\frac{g_{00}'}{g_{00}}\right) - \frac{1}{\eta^2}\left(6f_{00}f_{01} + f_{00}'^2 - \frac{f_{00}^2}{\eta^2}\right)$$

$$+ \frac{4}{\gamma-1}g_{00}^{(\gamma+1)}\left\{\eta^2\left[\gamma\left(2\frac{g_{02}}{g_{00}} - \frac{g_{01}^2}{g_{00}^2}\right) - f_{00}(4f_{01} - f_{00}^3)\right]\right.$$

$$\left. + \left(\gamma\frac{g_{01}}{g_{00}} - f_{00}^2\right)\left(\eta^2\left[(\gamma+1)\frac{g_{01}}{g_{00}} - f_{00}^2\right] + 1\right)\right\} \tag{16a}$$

b) Angle of attack

$$\xi^0, \epsilon: \quad f_{00}f_{10}'' = f_{10}'\left(f_{00}' + f_{00}\frac{g_{00}'}{g_{00}}\right) + \frac{4\eta^2}{\gamma-1}g_{00}^{(\gamma+1)}\left[\frac{\gamma}{2}\frac{g_{10}}{g_{00}}\right.$$

$$\left. - f_{00}(f_{10} + \tfrac{1}{2} - \delta)\right] \tag{13b}$$

$$\xi, \epsilon: \quad \left(\frac{2\gamma}{\gamma-1}\eta^2 g_{00}^{(\gamma+1)} - f_{00}^2\right)\left(\frac{g_{10}'}{g_{00}} - \frac{g_{10}g_{00}'}{g_{00}^2}\right) = -\left\{\frac{2\gamma}{\gamma-1}\eta^2 g_{00}^{(\gamma+1)}\right.$$

$$\times\left[2f_{00}(\delta - \tfrac{1}{2} - f_{10}) + (\gamma+1)\frac{g_{10}}{g_{00}}\right] - 4f_{00}f_{11}\right\}\frac{g_{00}'}{g_{00}} + 2f_{00}'f_{11}$$

$$+ 6f_{01}f_{10}' + \frac{1}{\eta}(4f_{00}f_{11} + 2f_{00}'f_{10}') - 2(f_{00}'f_{11} + f_{00}f_{11}')$$

$$- \frac{g_{10}}{g_{00}}f_{00}f_{00}' - 2f_{00}f_{10}'\frac{g_{01}}{g_{00}} + \frac{4\eta^2}{\gamma-1}g_{00}^{(\gamma+1)}\left[f_{00}f_{10}' + f_{00}'(f_{10} + \tfrac{1}{2} - \delta)\right]$$
$$\tag{14b}$$

- 24 -

$$\xi^2, \, \epsilon : \quad f_{00}f_{11}'' = -3f_{01}f_{10}'' - 2f_{11}f_{00}'' + f_{11}\left(f_{00}' + f_{00}\frac{g_{00}'}{g_{00}}\right) + f_{10}'\left[3f_{01}'\right.$$

$$+ f_{00}\left(\frac{g_{01}'}{g_{00}} - \frac{g_{01}g_{00}'}{g_{00}^2}\right) + 3f_{01}\frac{g_{00}'}{g_{00}} - 2f_{00}'\frac{g_{01}}{g_{00}}\right] + f_{00}'\left\{2f_{11}' + 2f_{11}\frac{g_{00}'}{g_{00}}\right.$$

$$+ f_{00}\left(\frac{g_{10}'}{g_{00}} - \frac{g_{10}g_{00}'}{g_{00}^2}\right) - f_{00}'\frac{g_{10}}{g_{00}} - 2f_{10}'\frac{g_{01}}{g_{00}}\right\} - \frac{1}{\eta^2}(4f_{00}f_{11} + 2f_{00}'f_{10}')$$

$$+ \frac{4}{\gamma-1}\,g_{00}^{(\gamma+1)}\left\{\eta^2\left[\frac{3}{2}\,\gamma\left(\frac{g_{11}}{g_{00}} - \frac{g_{01}g_{10}}{g_{00}^2}\right) - f_{00}(f_{11} - 3f_{00}^2f_{10}\right.\right.$$

$$+ 3(1+\delta)f_{00}^2) - 3f_{01}(f_{10} + \tfrac{1}{2} - \delta) - 2f_{00}f_{11}\right] + \left(\eta^2\left[(\gamma+1)\frac{g_{01}}{g_{00}}\right.\right.$$

$$\left.\left. - f_{00}^2\right] + 1\right)\left[\frac{\gamma}{2}\frac{g_{10}}{g_{00}} - f_{00}(f_{10} + \tfrac{1}{2} - \delta)\right] + \eta^2\left[2f_{00}(\delta - \tfrac{1}{2} - f_{10})\right.$$

$$\left.\left. + (\gamma+1)\frac{g_{10}}{g_{00}}\right]\left(\gamma\frac{g_{01}}{g_{00}} - f_{00}^2\right)\right\} \tag{15b}$$

$$\xi^3, \, \epsilon : \quad \left(\frac{2\gamma}{\gamma-1}\,\eta^2 g_{00}^{(\gamma+1)} - f_{00}^2\right)\left[\frac{g_{11}'}{g_{00}} - \frac{g_{01}g_{10}'}{g_{00}^2} - \frac{g_{10}g_{01}'}{g_{00}^2}\right.$$

$$\left. - \frac{g_{00}'}{g_{00}}\left(\frac{g_{11}}{g_{00}} - 2\frac{g_{01}g_{10}}{g_{00}^2}\right)\right] = -\left\{\frac{2\gamma}{\gamma-1}\,\eta^2 g_{00}^{(\gamma+1)}\left[2f_{00}(\delta - \tfrac{1}{2} - f_{10})\right.\right.$$

$$\left.\left. + (\gamma+1)\frac{g_{10}}{g_{00}}\right] - 4f_{00}f_{11}\right\}\left(\frac{g_{01}'}{g_{00}} - \frac{g_{01}g_{00}'}{g_{00}^2}\right) - \left\{\frac{2\gamma}{\gamma-1}\,g_{00}^{(\gamma+1)}\right.$$

$$\times\left[\eta^2\left(2[f_{01}(\delta - \tfrac{1}{2}) - (2\delta + \tfrac{1}{2})f_{00}^3 + 2f_{00}^3f_{10} - f_{00}f_{11} - f_{01}f_{10}]\right.\right.$$

$$+ 2(\gamma+1)\,\frac{g_{01}}{g_{00}}\,f_{00}(\delta - \tfrac{1}{2} - f_{10}) + (\gamma+1)\left(\frac{g_{11}}{g_{00}} + \gamma\,\frac{g_{01}g_{10}}{g_{00}^2}\right)$$

$$- (\gamma+1)f_{00}^2\,\frac{g_{10}}{g_{00}}\bigg) + 2f_{00}(\delta - \tfrac{1}{2} - f_{10}) + (\gamma+1)\,\frac{g_{10}}{g_{00}}\bigg] - 8f_{00}f_{12}$$

$$- 12f_{01}f_{11}\bigg\}\,\frac{g_{00}'}{g_{00}} - \bigg\{\frac{2\gamma}{\gamma-1}\,g_{00}^{(\gamma+1)}\left(\eta^2\left[(\gamma+1)\,\frac{g_{01}}{g_{00}} - f_{00}^2\right] + 1\right)$$

$$- 6f_{00}f_{01}\bigg\}\left(\frac{g_{10}'}{g_{00}} - \frac{g_{10}g_{00}'}{g_{00}^2}\right) + 12f_{00}'f_{12} + 2f_{01}'f_{11} + 6f_{01}f_{11}'$$

$$+ 20f_{02}f_{10}' + \frac{1}{\eta}(8f_{00}f_{12} + 12f_{01}f_{11} + 2f_{00}'f_{11}' + 2f_{01}'f_{10}')$$

$$- \frac{1}{\eta^3}(4f_{00}f_{11} + 2f_{00}'f_{10}') - 4(f_{00}'f_{12} + f_{00}f_{12}') - 6(f_{01}'f_{11}$$

$$+ f_{01}f_{11}') - 3f_{00}f_{00}'\left(\frac{g_{11}}{g_{00}} - \frac{g_{01}g_{10}}{g_{00}^2}\right) - \frac{g_{10}}{g_{00}}(f_{00}f_{01}' + 3f_{00}'f_{01})$$

$$- 2\,\frac{g_{01}}{g_{00}}(f_{00}f_{11}' + 3f_{01}f_{10}' + 2f_{00}'f_{11}) - f_{00}f_{10}'\left(4\,\frac{g_{02}}{g_{00}} - 2\,\frac{f_{01}^2}{g_{00}^2}\right)$$

$$+ \frac{4}{\gamma-1}\,g_{00}^{(\gamma+1)}\bigg\{\eta^2\left[f_{00}f_{11}' + f_{10}'(f_{01} - f_{00}^3) + f_{00}'[f_{11} - 3f_{00}^2 f_{10}\right.$$

$$+ 3(1+\delta)f_{00}^2] + f_{01}'(f_{10} + \tfrac{1}{2} - \delta)\bigg] + \left(\eta^2\left[(\gamma+1)\,\frac{g_{01}}{g_{00}} - f_{00}^2\right] + 1\right)$$

$$\times \left[f_{00}f_{10}' + f_{00}'(f_{10} + \tfrac{1}{2} - \delta)\right] + \eta^2 f_{00}f_{00}'\bigg[2f_{00}(\delta - \tfrac{1}{2} - f_{10})$$

$$+ (\gamma+1)\,\frac{g_{10}}{g_{00}}\bigg]\bigg\} \tag{14b}$$

Initial Conditions

    a) Zero angle

$$\xi^0, \epsilon^0 : \quad g_{00}(1) = 1 \tag{13c}$$

$$\xi, \epsilon^0 : \quad f_{00}(1) = 1 \; ; \; f'_{00}(1) = \frac{\gamma+1}{\gamma-1} \tag{14c}$$

$$\xi^2, \epsilon^0 : \quad g_{01}(1) = 0 \tag{15c}$$

$$\xi^3, \epsilon^0 : \quad f_{01}(1) = 0 \; ; \; f'_{01}(1) = 0 \tag{16c}$$

    b) Angle of attack

$$\xi^0, \epsilon : \quad f_{10}(1) = \tfrac{1}{2} + \delta \; ; \; f'_{10}(1) = \frac{\gamma+1}{\gamma-1} \tag{13d}$$

$$\xi, \epsilon : \quad g_{10}(1) = 0 \tag{14d}$$

$$\xi^2, \epsilon : \quad f_{11}(1) = -\tfrac{1}{2} \; ; \; f'_{11}(1) = 0 \tag{15d}$$

$$\xi^3, \epsilon : \quad g_{11}(1) = 0 \tag{16d}$$

The body condition, eq.(11), becomes

$$f_{00}(\eta_b)\xi + f_{01}(\eta_b)\xi^3 + 0(\xi^5) + \epsilon\left[f_{10}(\eta_b) + f_{11}(\eta_b)\xi^2 + 0(\xi^4)\right] + 0(\epsilon^2) = 0 \; . \tag{17a}$$

However, η_b is itself a function of ξ and depends parametrically on ϵ. Expanding $\eta_b(\xi; \epsilon)$ about its zero angle value yields

- 17 -

$$\eta_b(\xi; \epsilon) = \eta_b^{(0)}(\xi) + \epsilon \eta_b^{(1)}(\xi) + O(\epsilon^2). \tag{18a}$$

Using eq.(18), the functions of η_b in eq.(17a) may be expanded as follows

$$f_{00}(\eta_b) = f_{00}\left(\eta_b^{(0)}\right) + \epsilon \eta_b^{(1)} f_{00}'\left(\eta_b^{(0)}\right) + O(\epsilon^2)$$

$$f_{01}(\eta_b) = f_{01}\left(\eta_b^{(0)}\right) + \epsilon \eta_b^{(1)} f_{01}'\left(\eta_b^{(0)}\right) + O(\epsilon^2)$$

$$f_{10}(\eta_b) = f_{10}\left(\eta_b^{(0)}\right) + O(\epsilon)$$

$$f_{11}(\eta_b) = f_{11}\left(\eta_b^{(0)}\right) + O(\epsilon)$$

Eq.(17a) then becomes

$$f_{00}\left(\eta_b^{(0)}\right)\xi + f_{01}\left(\eta_b^{(0)}\right)\xi^3 + O(\xi^5) + \epsilon\left[f_{10}\left(\eta_b^{(0)}\right) + \eta_b^{(1)} f_{00}'\left(\eta_b^{(0)}\right)\xi \right.$$

$$\left. + f_{11}\left(\eta_b^{(0)}\right)\xi^2 + \eta_b^{(1)} f_{01}'\left(\eta_b^{(0)}\right)\xi^3 + O(\xi^4) \right] + O(\epsilon^2) = 0 \tag{17b}$$

Further expansion of $\eta_b^{(0)}(\xi)$ and $\eta_b^{(1)}(\xi)$ about $\xi = 0$ yields

$$\eta_b^{(0)}(\xi) = \eta_0^{(0)} + \eta_0^{(0)'}\,\xi + \eta_0^{(0)''}\,\frac{\xi^2}{2!} + O(\xi^3) \tag{19}$$

$$\eta_b^{(1)}(\xi) = \eta_0^{(1)} + \eta_0^{(1)'}\,\xi + \eta_0^{(1)''}\,\frac{\xi^2}{2!} + O(\xi^3) \tag{20}$$

- 18 -

where

$$\eta_0^{(0)} \equiv \eta_b^{(0)}(0)$$

$$\eta_0^{(1)} \equiv \eta_b^{(1)}(0)$$

and similar identities hold for the derivatives $\eta_0^{(0)'}$, $\eta_0^{(0)''}$, $\eta_0^{(1)'}$, $\eta_0^{(1)''}$. Then $f_{00}\left(\eta_b^{(0)}\right)$ may be expanded as

$$f_{00}\,\eta_b^{(0)} = f_{00}\left(\eta_0^{(0)}\right) + \left(\eta_0^{(0)'}\,\xi + \frac{\eta_0^{(0)''}}{2}\,\xi^2\right) f_{00}'\left(\eta^{(0)}\right)$$

$$+ \tfrac{1}{2}\eta_0^{(0)'2}\,\xi^2\,f_{00}''\left(\eta_0^{(0)}\right) + O(\xi^3)$$

with similar expansions holding for $f_{01}'\left(\eta_b^{(0)}\right)$, $f_{10}\left(\eta_b^{(0)}\right)$, $f_{00}'\left(\eta_b^{(0)}\right)$, $f_{11}\left(\eta_b^{(0)}\right)$, and $f_{01}'\left(\eta_b^{(0)}\right)$.

Putting these expansions into eq.(17b) yields

$$f_{00}\left(\eta_0^{(0)}\right)\xi + \eta_0^{(0)'}\,f_{00}'\left(\eta_0^{(0)}\right)\xi^2 + \left[\eta_0^{(0)''}\,f_{00}'\left(\eta_0^{(0)}\right) + \eta_0^{(0)'2}\,f_{00}''\left(\eta_0^{(0)}\right)\right.$$

$$\left. + 2f_{01}\left(\eta_0^{(0)}\right)\right]\xi^3/2 + O(\xi^4) + \epsilon\left\{f_{10}\left(\eta_0^{(0)}\right) + \left[\eta_0^{(0)'}\,f_{10}'\left(\eta_0^{(0)}\right)\right.\right.$$

$$\left. + \eta_0^{(1)}\,f_{00}'\left(\eta_0^{(0)}\right)\right]\xi + \left[\eta_0^{(1)'}\,f_{00}'\left(\eta_0^{(0)}\right) + \eta_0^{(1)}\,\eta_0^{(0)'}\,f_{00}''\left(\eta_0^{(0)}\right)\right.$$

$$\left. + f_{11}\left(\eta_0^{(0)}\right) + \frac{\eta_0^{(0)''}}{2}\,f_{10}'\left(\eta_0^{(0)}\right) + \frac{\eta_0^{(0)'2}}{2}\,f_{10}''\left(\eta_0^{(0)}\right)\right]\xi^2$$

$$+ \left[\eta_0^{(1)'}\,\eta_0^{(0)'}\,f_{00}''\left(\eta_0^{(0)}\right) + \tfrac{1}{2}\left\{\eta_0^{(1)''}\,f_{00}'\left(\eta_0^{(0)}\right) + \eta_0^{(1)}\left[\eta_0^{(0)''}\,f_{00}''\left(\eta_0^{(0)}\right)\right.\right.\right.$$

$$+ \eta_0^{(0)'2} \, f_{00}'''\left(\eta_0^{(0)}\right)\Big] + \eta_0^{(0)'} \, \eta_0^{(0)''} \, f_{10}''\left(\eta_0^{(0)}\right) + \frac{1}{3} \eta_0^{(0)'3} \, f_{10}'''\left(\eta_0^{(0)}\right)\Big\}$$

$$+ \eta_0^{(1)} \, f_{01}'\left(\eta_0^{(0)}\right) + \eta_0^{(0)'} \, f_{11}'\left(\eta_0^{(0)}\right)\Bigg] \xi^3 + O(\xi^4) + O(\epsilon^2) = 0 . \qquad (17c)$$

Since this equation must hold for all ξ and ϵ , equating coefficients of like powers of ξ and ϵ yields

$$f_{00}\left(\eta_0^{(0)}\right) = 0 \qquad\qquad (14e)$$

$$f_{10}\left(\eta_0^{(0)}\right) = 0 \qquad\qquad (13e)$$

$$\eta_0^{(0)'} \, f_{00}'\left(\eta_0^{(0)}\right) = 0 \qquad\qquad (21a)$$

$$\eta_0^{(1)} \, f_{00}'\left(\eta_0^{(0)}\right) = 0 \qquad\qquad (21b)$$

$$\eta_0^{(0)''} \, f_{00}'\left(\eta_0^{(0)}\right) + 2f_{01}\left(\eta_0^{(0)}\right) = 0 \qquad\qquad (21c)$$

$$\eta_0^{(1)'} \, f_{00}'\left(\eta_0^{(0)}\right) + f_{11}\left(\eta_0^{(0)}\right) + \eta_0^{(0)''} \, \frac{f_{10}'\left(\eta_0^{(0)}\right)}{2} = 0 \qquad\qquad (21d)$$

$$\eta_0^{(1)''} \, f_{00}'\left(\eta_0^{(0)}\right) = 0 \qquad\qquad (21e)$$

Eq.(14e) is the condition used to terminate the integration in any truncation and determines $\eta_0^{(0)}$, the value of η at the nose of the zero-angle body. Since $\eta_0^{(0)}$ is thus determined, eq.(13e) is the condition that determines δ , i.e., this condition is satisfied for only one value of δ in the initial-condition eq.(13d) and differential eqs.(13b), (14b), (15b), and (16b).

- 20 -

Eqs.(21a) - (21e), along with eqs.(18), (19), and (20), determine
the body shape. Eq.(21a) yields $\eta_0^{(0)'} = 0$. This indicates that the
zero-angle body is represented by an even series in powers of ξ . The
same conclusion could have been reached from symmetry considerations.
Eq.(21b) yields $\eta_0^{(1)} = 0$, i.e., there is no perturbation to the zero-
angle body at its nose to this order of analysis. Eqs.(21c) and (21d)
determine $\eta_0^{(0)''}$, $\eta_0^{(1)'}$, in terms of the values of the functions of
η and their derivatives evaluated at $\eta_0^{(0)}$. Eq.(21e) yields
$\eta_0^{(1)''} = 0$, which indicates that the angle-of-attack perturbation to
the body is represented by an odd series in powers of ξ .

Thus, it is seen that the condition $\psi(\eta_b) = 0$ determines not
only the body shape, but also the unknown quantity δ .

Eqs.(13a) - (13e), and (14a) - (14e) comprise the first-truncation
problem. Eqs.(13a), (14a), (13c), (14c), and (14e) define the zero-
angle problem, whereas eqs.(13b), (14b), (13d), (14d), and (13e) define
the angle of attack problem. Note that the zero-angle differential
equations (13a) and (14a) are nonlinear and that eq.(14a) contains g_{01}' ,
as previously mentioned. Setting g_{01} equal to zero allows the zero-
angle problem to be solved. Setting f_{01}, f_{11} , and g_{01} equal to
zero in eqs.(13b) and (14b), and utilizing the zero-angle results,
initial condition eqs.(13d) and (14d), and body-condition eq.(13e)
allows solution of the first-truncation equations for the angle-of-
attack problem.

Similar remarks apply to the second-truncation problem defined by
eqs.(13a) - (13e), (14a) - (14e), (15a) - (15e), and (16a) - (16e), with
functions having a second subscript of 1 being retained and those
having a second subscript of 2 being set equal to zero. Higher-order
problems are solved in like manner.

2. Three-Dimensional Flow

In contrast to the case of plane flow, the continuity equation is
satisfied by the introduction of a pair of stream functions, ψ_1 and
ψ_2 according to

$$\rho \vec{q} = \nabla \psi_1 \times \nabla \psi_2 \qquad (22)$$

The use of such a pair of functions in this manner was introduced by Clebsch [9].

The entropy-conservation equation, (5e), then states that

$$\frac{p}{\rho^\gamma} = g(\psi_1, \psi_2) \qquad (23)$$

where the functional form of g is to be determined from the boundary conditions at the shock wave.

Using equations (22) and (23) in equations (5b), (5c), and (5d) yields the following equations for ψ_1, ψ_2, and ρ :

$$(\psi_{1\eta}\psi_{2\varphi} - \psi_{1\varphi}\psi_{2\eta}) \left[\psi_{1\xi\eta}\psi_{2\varphi} + \psi_{1\eta}\psi_{2\xi\varphi} - \psi_{1\xi\varphi}\psi_{2\eta} - \psi_{1\varphi}\psi_{2\xi\eta} \right.$$

$$\left. - (\psi_{1\eta}\psi_{2\varphi} - \psi_{1\varphi}\psi_{2\eta}) \left(\frac{\rho_\xi}{\varphi} + \frac{h_{2\xi}}{h_2} + \frac{h_{3\xi}}{h_3} \right) \right] + (\psi_{1\varphi}\psi_{2\xi} - \psi_{1\xi}\psi_{2\varphi})$$

$$\times \left[\psi_{1\eta\eta}\psi_{2\varphi} + \psi_{1\eta}\psi_{2\eta\varphi} - \psi_{1\eta\varphi}\psi_{2\eta} - \psi_{1\varphi}\psi_{2\eta\eta} - (\psi_{1\eta}\psi_{2\varphi} - \psi_{1\varphi}\psi_{2\eta}) \right.$$

$$\left. \times \left(\frac{\rho_\eta}{\rho} + \frac{h_{2\eta}}{h_2} + \frac{h_{3\eta}}{h_3} \right) \right] + (\psi_{1\xi}\psi_{2\eta} - \psi_{1\eta}\psi_{2\xi}) \left[\psi_{1\eta\varphi}\psi_{2\varphi} + \psi_{1\eta}\psi_{2\varphi\varphi} - \psi_{1\varphi\varphi}\psi_{2\eta} \right.$$

$$\left. - \psi_{1\varphi}\psi_{2\eta\varphi} - (\psi_{1\eta}\psi_{2\varphi} - \psi_{1\varphi}\psi_{2\eta}) \frac{\rho_\varphi}{\rho} \right] + \frac{\eta}{c\xi^2 + \eta^2} (\psi_{1\eta}\psi_{2\varphi} - \psi_{1\varphi}\psi_{2\eta})(\psi_{1\varphi}\psi_{2\xi}$$

$$- \psi_{1\xi}\psi_{2\varphi}) - \left[\frac{c\xi}{(c\xi^2 + \eta^2)} \frac{h_2^2}{h_1^2} (\psi_{1\varphi}\psi_{2\xi} - \psi_{1\xi}\psi_{2\varphi})^2 + \frac{h_3^2}{\xi h_1^2} (\psi_{1\xi}\psi_{2\eta} - \psi_{1\eta}\psi_{2\xi})^2 \right]$$

- 32 -

$$+ h_2^2 \, h_3^2 \, \rho^{(\gamma+1)} \left[g_{\psi 1} \psi_{1\xi} + g_{\psi 2} \psi_{2\xi} + \gamma \, \frac{\rho_\xi}{\rho} \, g(\psi_1, \psi_2) \right] = 0 \qquad (24a)$$

$$(\psi_{1\eta} \psi_{2\varphi} - \psi_{1\varphi} \psi_{2\eta}) \left[\psi_{1\xi\varphi} \psi_{2\xi} + \psi_{1\varphi} \psi_{2\xi\xi} - \psi_{1\xi\xi} \psi_{2\varphi} - \psi_{1\xi} \psi_{2\xi\varphi} - (\psi_{1\varphi} \psi_{2\xi} - \psi_{1\xi} \psi_{2\varphi}) \right.$$

$$\left. \times \left(\frac{\rho_\xi}{\rho} + \frac{h_{1\xi}}{h_1} + \frac{h_{3\xi}}{h_3} \right) \right] + (\psi_{1\varphi} \psi_{2\xi} - \psi_{1\xi} \psi_{2\varphi}) \left[\psi_{1\eta\varphi} \psi_{2\xi} + \psi_{1\varphi} \psi_{2\eta\xi} - \psi_{1\xi\eta} \psi_{2\varphi} \right.$$

$$\left. - \psi_{1\xi} \psi_{2\eta\varphi} - (\psi_{1\varphi} \psi_{2\xi} - \psi_{1\xi} \psi_{2\varphi}) \left(\frac{\rho_\eta}{\rho} + \frac{h_{1\eta}}{h_1} + \frac{h_{3\eta}}{h_3} \right) \right] + (\psi_{1\xi} \psi_{2\eta} - \psi_{1\eta} \psi_{2\xi})$$

$$\times \left[\psi_{1\varphi\varphi} \psi_{2\xi} + \psi_{1\varphi} \psi_{2\xi\varphi} - \psi_{1\xi} \psi_{2\varphi\varphi} - \psi_{1\xi\varphi} \psi_{2\varphi} - (\psi_{1\varphi} \psi_{2\xi} - \psi_{1\xi} \psi_{2\varphi}) \frac{\rho_\varphi}{\rho} \right]$$

$$+ \frac{C\xi}{C\xi^2 + \eta^2} (\psi_{1\eta} \psi_{2\varphi} - \psi_{1\varphi} \psi_{2\eta})(\psi_{1\varphi} \psi_{2\xi} - \psi_{1\xi} \psi_{2\varphi}) - \left[\frac{\eta}{C\xi^2 + \eta^2} \frac{h_1^2}{h_2^2} (\psi_{1\eta} \psi_{2\varphi} - \psi_{1\varphi} \psi_{2\eta})^2 \right.$$

$$\left. + \frac{h_3^2}{\eta h_2^2} (\psi_{1\xi} \psi_{2\eta} - \psi_{1\eta} \psi_{2\xi})^2 \right] + h_1^2 \, h_3^2 \, \rho^{(\gamma+1)} \left[g_{\psi 1} \psi_{1\eta} + g_{\psi 2} \psi_{2\eta} + \gamma \, \frac{\rho_\eta}{\rho} \, g(\psi_1, \psi_2) \right] = 0$$

$$(24b)$$

$$(\psi_{1\eta} \psi_{2\varphi} - \psi_{1\varphi} \psi_{2\eta}) \left[\psi_{1\xi} \psi_{2\xi\eta} + \psi_{1\xi\xi} \psi_{2\eta} - \psi_{1\xi\eta} \psi_{2\xi} - \psi_{1\eta} \psi_{2\xi\xi} - (\psi_{1\xi} \psi_{2\eta} - \psi_{1\eta} \psi_{2\xi}) \right.$$

$$\left. \times \left(\frac{\rho_\xi}{\rho} + \frac{h_{1\xi}}{h_1} + \frac{h_{2\xi}}{h_2} \right) \right] + (\psi_{1\varphi} \psi_{2\xi} - \psi_{1\xi} \psi_{2\varphi}) \left[\psi_{1\xi\eta} \psi_{2\eta} + \psi_{1\xi} \psi_{2\eta\eta} \right.$$

$$\left. - \psi_{1\eta\eta} \psi_{2\xi} - \psi_{1\eta} \psi_{2\xi\eta} - (\psi_{1\xi} \psi_{2\eta} - \psi_{1\eta} \psi_{2\xi}) \left(\frac{\rho_\eta}{\rho} + \frac{h_{1\eta}}{h_1} + \frac{h_{2\eta}}{h_2} \right) \right] + (\psi_{1\xi} \psi_{2\eta}$$

$$\left. - \psi_{1\eta} \psi_{2\xi}) \left[\psi_{1\xi\varphi} \psi_{2\eta} + \psi_{1\xi} \psi_{2\eta\varphi} - \psi_{1\eta\varphi} \psi_{2\xi} - \psi_{1\eta} \psi_{2\xi\varphi} - (\psi_{1\xi} \psi_{2\eta} - \psi_{1\eta} \psi_{2\xi}) \frac{\rho_\varphi}{\rho} \right] \right.$$

- 23 -

$$+ (\psi_{1\xi}\psi_{2\eta} - \psi_{1\eta}\psi_{2\xi}) \left[\frac{1}{\xi} (\psi_{1\eta}\psi_{2\varphi} - \psi_{1\varphi}\psi_{2\eta}) + \frac{1}{\eta} (\psi_{1\varphi}\psi_{2\xi} - \psi_{1\xi}\psi_{2\varphi}) \right]$$

$$+ h_1^2 h_2^2 \rho^{(\gamma+1)} \left[g_{\psi 1}\psi_{1\varphi} + g_{\psi 2}\psi_{2\varphi} + \gamma \frac{\rho_\varphi}{\rho} g(\psi_1, \psi_2) \right] = 0 \qquad (24c)$$

Before the initial conditions are presented, a few words are in order regarding the stream functions ψ_1 and ψ_2. These functions possess a degree of arbitrariness in that it is only required that the surfaces $\psi_1(\xi, \eta, \varphi) = $ constant and $\psi_2(\xi, \eta, \varphi) = $ constant be stream surfaces, that is, surfaces in which streamlines are imbedded. The intersections of these surfaces are then streamlines. If one considers a uniform stream for simplicity, there are any number of pairs of surfaces which can be set up to satisfy this requirement. For example, one such pair consists of orthogonal or skewed planes. Another is concentric circular cylinders and orthogonal planes through the common axis of the cylinders. If, however, one considers axisymmetric flow in a (ξ, η, φ) coordinate system and chooses for ψ_2 the azimuthal angular coordinate φ, ψ_1 is the familiar Stokes stream function. Hence, since we are considering small angle of attack, it is reasonable to perturb ψ_2 about φ and ψ_1 about the Stokes function.

Consider Fig.2. Depicted there is a shock wave that is a paraboloid of revolution at angle ϵ to the uniform free stream. A line at angle ϵ through a known point on the x-axis (e.g., central point of a hyperboloid, focus of a paraboloid, center of a sphere, point of intersection of major and minor axes of an ellipsoid) is chosen as reference from which the distance to the body streamline ahead of the shock is measured. Concentric circular cylinders about $\psi_1 = 0$ and planes of angle $\beta = $ constant are chosen for the stream surfaces ahead of the shock (see section A-A, Fig.2). With ψ_1 and ψ_2 defined in this manner, the initial conditions are

$$\rho = \frac{(\gamma + 1)M^2(1 - B\xi^2 - 2\epsilon\xi\sqrt{1 - B\xi^2}\cos\varphi)}{(\gamma - 1)M^2(1 - B\xi^2 - 2\epsilon\xi\sqrt{1 - B\xi^2}\cos\varphi) + 2(1 + C\xi^2)} \tag{25a}$$

$$\psi_1 = \xi^2/2 + \epsilon\xi\cos\varphi\left(\frac{\sqrt{1 - B\xi^2}}{B} + \delta\right) \tag{25b}$$

$$\psi_2 = \varphi - \frac{\epsilon}{\xi}\sin\varphi\left(\frac{\sqrt{1 - B\xi^2}}{B} + \delta\right) \tag{25c}$$

$$\psi_{1\eta} = \rho\xi\sqrt{1 - B\xi^2}\left[\xi + \epsilon\cos\varphi\left(1 + \delta + \frac{\sqrt{1 - B\xi^2}}{B}\right)\right] \tag{25d}$$

$$\psi_{2\eta} = \frac{\epsilon\rho\sin\varphi}{\xi}\left[(1 - B\xi^2)\left(\frac{\sqrt{1 - B\xi^2}}{B} + \delta + \frac{\xi^2}{\sqrt{1 - B\xi^2}}\right)\right.$$
$$\left. - (1 + C\xi^2)\right] \tag{25e}$$

at $\eta = 1$.

and the function $g(\psi_1, \psi_2)$ is

$$g(\psi_1, \psi_2) = \left(2\gamma M^2 \left\{ 1 - B\left[2\psi_1 - 2\sqrt{2\psi_1} \ \epsilon \cos \psi_2 \left(\frac{\sqrt{1 - 2B\psi_1}}{B} + \delta \right) \right] \right.\right.$$

$$\left. - 2\sqrt{2\psi_1} \ \epsilon \cos \psi_2 \sqrt{1 - 2B\psi_1} \right\}$$

$$\left. \frac{- (\gamma-1)\left\{ 1 + (1-B)\left[2\psi_1 - 2\sqrt{2\psi_1} \ \epsilon \cos \psi_2 \left(\frac{\sqrt{1 - 2B\psi_1}}{B} + \delta \right) \right\} \right\}}{\gamma(\gamma+1)M^2 \left\{ 1 + (1-B)\left[2\psi_1 - 2\sqrt{2\psi_1} \ \epsilon \cos \psi_2 \left(\frac{\sqrt{1 - 2B\psi_1}}{B} + \delta \right) \right] \right\}} \right)$$

$$\times \left[\frac{(\gamma-1)M^2\left\{ 1 - B\left[2\psi_1 - 2\sqrt{2\psi_1} \ \epsilon \cos \psi_2 \left(\frac{\sqrt{1 - 2B\psi_1}}{B} + \delta \right) \right] - 2\sqrt{2\psi_1} \ \epsilon \cos \psi_2 \sqrt{1 - 2B\psi_1} \right\} + 2\left\{ 1 + (1-B)\left[2\psi_1 - 2\sqrt{2\psi_1} \ \epsilon \cos \psi_2 \left(\frac{\sqrt{1 - 2B\psi_1}}{B} + \delta \right) \right] \right\}}{(\gamma+1)M^2 \left\{ 1 - B\left[2\psi_1 - 2\sqrt{2\psi_1} \ \epsilon \cos \psi_2 \left(\frac{\sqrt{1 - 2B\psi_1}}{B} + \delta \right) \right] - 2\sqrt{2\psi_1} \ \epsilon \cos \psi_2 \sqrt{1 - 2B\psi_1} \right\}} \right]^{\gamma}$$

(26a)

For the special case of a paraboloidal shock $(B = 0, \ C = 1)$ the shift in reference line previously mentioned on page 9 results in

$$\cdot) = \frac{(\gamma + 1)M^2(1 - 2\epsilon\xi \cos \varphi)}{(\gamma - 1)M^2(1 - 2\epsilon\xi \cos \varphi) + 2(1 + \xi^2)} \tag{25f}$$

$$\psi_1 = \xi^2/2 + \epsilon\xi \cos \varphi \left(\frac{1 - \xi^2}{2} + \delta \right) \tag{25g}$$

$$\psi_2 = \varphi - \frac{\epsilon \sin \varphi}{\xi} (\delta + \tfrac{1}{2} - \xi^2/2) \tag{25h}$$

$$\psi_{1\eta} = \rho\xi \left[\xi + \epsilon \cos \varphi \left(\frac{3}{2} + \delta - \xi^2/2 \right) \right] \tag{25i}$$

$$\psi_{2\eta} = \frac{\epsilon\rho \sin \varphi}{\xi} (\delta - \tfrac{1}{2} - \xi^2/2) \tag{25j}$$

$$g(\psi_1, \psi_2) = \frac{\left(2\gamma M^2 (1 - 2\sqrt{2\psi_1}\, \epsilon \cos \psi_2) - (\gamma-1) \left[1 + 2\psi_1 - 2\sqrt{2\psi_1}\, \epsilon \cos \psi_2 (\delta + \tfrac{1}{2} - \psi_1) \right] \right)}{\gamma(\gamma+1)M^2 \left[1 + 2\psi_1 - 2\sqrt{2\psi_1}\, \epsilon \cos \psi_2 (\delta + \tfrac{1}{2} - \psi_1) \right]}$$

$$\times \left[\frac{(\gamma-1)M^2(1-2\sqrt{2\psi_1}\, \epsilon \cos \psi_2) + 2 \left[1+2\psi_1 - 2\sqrt{2\psi_1}\, \epsilon \cos \psi_2 (\delta + \tfrac{1}{2} - \psi_1) \right]}{(\gamma+1)M^2(1 - 2\sqrt{2\psi_1}\, \epsilon \cos \psi_2)} \right]^{\gamma} \tag{26b}$$

The boundary condition at the body is

$$\psi_1 = 0 \quad \text{at} \quad \eta = \eta_b \tag{27}$$

The method of solution is essentially the same as for plane flow. Separate variables by setting

$$2\psi_1 = f_{00}(\eta)\xi^2 + f_{01}(\eta)\xi^4 + f_{02}(\eta)\xi^6 + O(\xi^8)$$

$$+ \epsilon \cos \varphi \left[f_{10}(\eta)\xi + f_{11}(\eta)\xi^3 + f_{12}(\eta)\xi^5 + O(\xi^7) \right] + O(\epsilon^2) \tag{28a}$$

- 27 -

$$\psi_2 = \varphi + \epsilon \sin \varphi \left[\frac{h_{10}(\eta)}{\xi} + h_{11}(\eta)\xi + h_{12}(\eta)\xi^3 + \epsilon\xi^5) \right] + O(\epsilon^2) \tag{28b}$$

$$\frac{\gamma-1}{\gamma+1} \rho = g_{00}(\eta) + g_{01}(\eta)\xi^2 + g_{02}(\eta)\xi^4 + O(\xi^6)$$

$$+ \epsilon \cos \varphi \left[g_{10}(\eta)\xi + g_{11}(\eta)\xi^3 + g_{12}(\eta)\xi^5 + O(\xi^7) \right] + O(\epsilon^2) \tag{28c}$$

Again, after one substitutes these expansions into eqs.(24) - (27) and equates coefficients of like powers of ξ and ϵ, the series must be truncated to obtain a solution. As in the plane-flow case, the equations for f_{00} and g_{00} are nonlinear and succeeding equations for the other unknown functions of η are linear, with the equations for the angle-of-attack functions having variable coefficients depending on the zero-angle solution. The body boundary condition, eq.(27), is applied in a similar manner as outlined for plane flow with the modification that the body shape is now given by

$$\eta_b(\xi,\varphi; \epsilon) = \eta_b^{(0)}(\xi) + \epsilon \cos \varphi \, \eta_b^{(1)}(\xi) \tag{18b}$$

3. Sonic Lines and Surface Pressure Distributions

In addition to body shapes, sonic lines and surface pressure distributions out to the sonic line were calculated to investigate convergence of the series expansions away from the axis. The mathematical details of obtaining these quantities will now be presented.

The energy-conservation equation for a perfect gas,

$$\frac{\gamma}{\gamma-1} \frac{\bar{p}}{\bar{\rho}} + \frac{\bar{q}^2}{2} = \frac{\gamma}{\gamma-1} \frac{\bar{p}_\infty}{\bar{\rho}_\infty} + \frac{\bar{q}_\infty^2}{2} \tag{29}$$

where barred quantities represent dimensional physical quantities,

becomes, after suitable nondimensionalization

$$M_\ell^2 = \frac{2}{\gamma - 1}\left[\frac{2 + (\gamma - 1)M^2}{2\gamma M^2}\frac{\rho}{p} - 1\right] \tag{30}$$

where M_ℓ is the local Mach number of the flow in the shock layer. On the sonic line, the local Mach number is unity. Furthermore, the mass- and entropy-conservation equations yield $p = \rho^\gamma f(\psi)$ (plane flow), and $p = \rho^\gamma g(\psi_1, \psi_2)$ (three-dimensional flow). Putting this information into eq. (30) yields

$$\frac{2 + (\gamma - 1)M^2}{2\gamma M^2}\frac{\rho^{(1-\gamma)}}{f(\psi)} = \frac{\gamma + 1}{2} \qquad (\nu = 0) \tag{31a}$$

$$\frac{2 + (\gamma - 1)M^2}{2\gamma M^2}\frac{\rho^{(1-\gamma)}}{g(\psi_1, \psi_2)} = \frac{\gamma + 1}{2} \qquad (\nu = 1) \tag{31b}$$

Introduction of f or g in terms of the series expansions for ψ, ψ_1, and ψ_2 yields equations which, for a given truncation, are algebraic expressions for ξ in terms of functions of η. Selection of values of η between the shock and body allows corresponding values of ξ to be calculated, thus determining points on the sonic line.

The equations for surface pressure distributions are obtained by utilizing

$$p = \rho^\gamma f(\psi) \qquad (\nu = 0) \tag{7}$$

$$p = \rho^\gamma g(\psi_1, \psi_2) \qquad (\nu = 1). \tag{23}$$

Again, substituting appropriate expansions for ρ, f, and g yields $p(\xi, \eta; \epsilon)$. Use of known pairs of values of ξ and η on the body allows the pressure to be calculated in any given truncation.

- 29 -

III. RESULTS AND DISCUSSION

A. Zero Angle of Attack

To examine the convergence of the series expansions for the stream
functions and density, zero-angle-of-attack results will be presented
initially. From consideration of the simplifications brought about
in the equations and boundary conditions, the free stream Mach number
is taken to be infinite and the shock shape to be a portion of a circle,
parabola, sphere and paraboloid of revolution. The specific heat ratio,
γ , is taken to be 1.4.

The first four truncations have been carried out for the circular
and paraboloidal shock, while the first three truncations have been cal-
culated for the spherical and parabolic shock waves. The numerical
integration of the ordinary differential equations for the unknown
functions of η was accomplished using a fourth-order Runge-Kutta-Gill
method [10]. The computations were carried out on an IBM 7090 electronic
computing machine at Lockheed Missiles and Space Company, Sunnyvale,
California. Machine times of two to three minutes were required for
each case.

Results on and away from the axis are compared with numerical
solutions obtained using the inverse method developed by Van Dyke [1]
and refined by Fuller [11]. Convergence on the axis is extremely rapid,
three truncations giving the stagnation-point density correct to five
significant figures and the standoff distance to four significant figures
as determined by comparison of the parabolic shock solution with
Garabedian's results [12]. Convergence off the axis is somewhat less
rapid, as is to be expected from the form of the expansions. The term
convergence is used here in the sense that, whenever two successive
truncations yield values for a physical quantity identical in three or
more significant figures, it is said that the quantity has converged.
Nothing can be said about convergence of the assumed series in the strict
mathematical sense, since the functional form of the series coefficients
is not explicitly known.

1. Plane Flow

Results for the circular and parabolic shock waves are given in
Figures 3 - 6 and 11. Figures 3 - 5 apply to the circular shock. In
Figure 3, the convergence of the reduced stream function ψ/ξ , and
the density function, $(\gamma-1)\rho/(\gamma+1)$, along the axis ($\xi = 0$) is
examined and results of one, two, three, and four truncations compared
with numerical solutions. As previously mentioned, convergence is
extremely rapid for both the density and stream function, the differ-
ences between the second, third and fourth truncations being indiscern-
ible to the scale of the plot. The standoff distance referred to the
shock nose radius, Δ/R_s , is determined to be 0.1895 by the second
truncation and 0.1899 by the third and fourth truncations. This con-
verged result is smaller than the value of 0.1912 determined by NASA
case MDF*, and larger than the value of 0.1880 determined by NASA case
34 (these values for standoff distance are obtained using that value
of η at which f_{oc} goes to zero, along with eq. (2d)). The method
of solution for NASA case MDF contains a smoothing process [11] whereas
that for case 34 does not. As pointed out in ref. [11], the smoothing
process has the effect of increasing standoff distance. Comparison of
the two NASA results with the converged value leads to the conclusion
that the NASA data are not sufficiently accurate to be used as an
absolute basis of comparison. This point will be further borne out as
other physical quantities are considered.

Figure 4 compares sonic lines and body shapes as determined from
the second, third, and fourth truncations with the results of NASA case
MDF. The sonic line determined by the first truncation is a circle
having a radius of 1.593 and center at $x = 1, r = 0$, while the first
truncation body determined by the numerical integration is the point
$x = 1, r = 0$. Note that the first-truncation sonic line lies ahead
of the shock. This result is obtained by analytic continuation of the
solution upstream of the shock wave and is, of course, physically

---

* NASA results for cases MDF, MDD, RS1 and RS4 courtesy of Ames
  Aeronautical Laboratory (unpublished).

- 31 -

unrealizable since the flow ahead of the shock is uniform at infinite Mach number. Comparison of the body shapes determined by the third and fourth truncations indicates convergence beyond the sonic point to a shape other than the NASA result. The sonic line, however, has not converged and higher truncations would be required to determine its exact location.

Figure 5 compares the surface pressure distribution determined by the second, third, and fourth truncations with the NASA results. Convergence has been obtained for about two-thirds of the distance to the sonic point. The converged portion of the curve and the NASA results are parallel, but do not coincide due to the discrepancy in body position. Higher truncations are required to obtain convergence all the way to the sonic point, but the trend indicates that the converged values will probably not parallel the NASA data for the entire distance.

Figures 6 and 11 apply to a parabolic shock. The results of one, two, and three truncations for the reduced stream function and density function along the axis are compared with both NASA results and Garabedian's solution [12] in Figure 6. Results for the circular shock have indicated that the NASA data lack sufficient accuracy to be used as an absolute basis for comparison and that the method under consideration possesses internal consistency. The question of convergence to the correct solution may be answered by comparison with Garabedian's result for a parabolic shock at infinite free stream Mach number. Garabedian claims 1/10 of one percent accuracy for his standoff distance of 0.18516. The third truncation yields a standoff distance of 0.18514, thus indicating at least three and perhaps four significant figure accuracy for this quantity.

Figure 11 compares body shape and sonic lines as determined by one, two, and three truncations with NASA results. For this case, comparison indicates near convergence of the third truncation for both quantities.

2. Axisymmetric Flow

Results for spherical and paraboloidal shock waves are given in
Figures 7 - 10. Figure 7 depicts the variation of the reduced stream
function, $2\psi/\xi^2$, and density function along the axis of symmetry
between a spherical shock and the body. Again, the convergence is
extremely rapid, three truncations giving a standoff distance, Δ/R_s ,
of 0.0998 compared with the NASA results of 0.0981 (unsmoothed) and
0.0993 (smoothed).

Figures 8 - 10 apply to a paraboloidal shock wave. Figure 8 yields
a standoff distance of 0.8956 as determined by the second, third, and
fourth truncations. Hence, the standoff distance converges to four
significant figures in only two truncations for this case.

Figure 9 compares body shapes and sonic lines with a NASA numerical
solution. In the first truncation, both body and sonic lines are
η = constant lines, the body being at η = 0.8552 and the sonic line
at η = 1.0780. The corresponding values of x and r may be obtained
from eqs.(2b) and (2c). Again, the first-truncation sonic line lies
ahead of the shock, this result having been obtained by analytic con-
tinuation of the solution upstream of the shock wave. Since the sonic
point on the body has a ξ coordinate greater than in the case of the
circular shock, neither the body shape nor the sonic line appears con-
verged even in four truncations for this case. However, consider the
surface pressure distribution given in Figure 10. One-dimensional
streamtube relations yield the result that, for $\gamma = 1.4$, the pressure
at the sonic point on the body must have the value 0.486. This value is
plotted at the value of x determined by the intersection of the fourth-
truncation body and sonic line from Figure 9 (asterisk symbol, Figure
10). One sees that this point nearly coincides with the pressure curve
obtained by applying a Shank's transformation [13] to the fourth-
truncation pressure series. The nonlinear Shank's transformation
causes the slowly convergent pressure series to converge more rapidly.
The above agreement indicates near convergence without the necessity
of calculating the fifth truncation.

B. Small Angle of Attack

The analysis outlined for the angle-of-attack problem has been carried out for shock waves that are parabolas (plane flow) and paraboloids of revolution (three-dimensional flow). The first three truncations have been calculated for each shock shape. The free stream Mach number is taken to be infinite, and γ takes on the values 1.4, 1.2, 1.1, 1.05. The resulting body shapes, sonic lines, and positions of the body streamlines at their points of intersection with the shock wave are shown in Figures 12 and 13 for $\epsilon = 10^{\circ}$, $\gamma = 1.4$, where a finite value of ϵ has been selected for graphical purposes and the error is $O(\epsilon^2)$. For purpose of comparison, body shapes and sonic lines for a parabolic and paraboloidal shock at zero angle are given in Figures 11 and 9 respectively. Computing machine times of five to six minutes per case were required since the zero-angle functions appear as coefficients in the angle-of-attack equations and hence must be stored in the machine. Also, in certain cases it was necessary to use very small step sizes (e.g., $\Delta\eta = 10^{-4}$) in order to obtain accurate values for the quantity δ .

Of particular interest in the angle-of-attack problem is whether or not the streamline that wets the body crosses the shock normally, thus having maximum entropy. For this to be so, the quantity δ (see Figure 2) must have the value $\frac{1}{2}$. The results of the analyses are given in Table I.

TABLE I

Values of δ

	Parabolic Shock, $M = \infty$				Paraboloidal Shock, $M = \infty$			
	γ				γ			
Truncation	1.4	1.2	1.1	1.05	1.4	1.2	1.1	1.05
1	1518	8417	-	-	88.00	37.48	25.79	-1.34
2	.4838	.4935	.4974	.4990	.5576	.5394	.5190	.5042
3	.4748	.4908	.4966	.4988	.4871	.4950	.4984	.5004

For all cases the trend of decreasing δ with increasing truncation is toward a value of δ slightly less than $\frac{1}{2}$. For the three-dimensional case, a reversal of this trend in higher truncations could conceivably result in a value of $\frac{1}{2}$. However, even if this reversal took place in two dimensions, a converged value would be expected to lie between the second-and third-truncation values and thus could never be $\frac{1}{2}$. Hence, the streamline that wets the body passes through the shock wave slightly above the point where it is a normal shock. However, as the Newtonian limit process ($M \to \infty$, $\gamma \to 1$) is carried out, the trend is toward a value of $\frac{1}{2}$. Hence in this limit, when the parabolic and paraboloidal shock and body coincide, the body is covered by the maximum-entropy streamline in both the plane and three-dimensional cases.

Since the shock waves possess symmetry about the x-axis, the resulting body shapes are asymmetric to this axis. Consideration of the comparison in Figure 11 of the third-truncation body for the parabolic shock at zero angle with the NASA results, and of the results for the circular shock given in Figure 4, lead to the conclusion that, for symmetric plane flow at $M = \infty$, three truncations yield a nearly converged body out to the sonic point. Since ϵ is taken as small, it is reasonable to extend this conclusion to include small angles of incidence. With the above facts in mind, and the realization that it is somewhat impractical to talk about asymmetric shapes from an experimental or engineering viewpoint, an attempt was made to find an axis system in which that portion of the two-dimensional body given by the third-truncation (Figure 12) out to the sonic points could be closely approximated by a conic section. An ellipse was fitted by a trial-and-error procedure in which the positions of the foci and major axis were varied until points on the ellipse and third truncation body coincided to three significant figures (Figure 14). The ellipse is given by the equation $\bar{x}^2/0.37 + \bar{r}^2/0.28 = 1$, where the origin of the ($\bar{x}$, $\bar{r}$) axes is at $x = .090$, $r = - .033$, and the $\bar{x}$ axis is at angle 14.20^{0} measured clockwise from the free stream direction. Thus, the shock wave is seen to rotate about 0 per cent as fast as the body as the angle of attack is imposed.

No attempt was made to perform a corresponding fit to the three-dimensional body determined by the third truncation, since Figure 9 indicates that the body shape out to the sonic point has not converged. Note, however, that the third-truncation body is closer to the shock in the $\varphi = \pi$ plane than in the $\varphi = 0$ plane. Hence, to this truncation, the shock wave still must rotate more slowly than the body as angle of attack is imposed.

IV. CONCLUSIONS

A semi-analytical, semi-numerical method of analysis has been developed and successfully applied to the problem of two-and three-dimensional hypersonic flow past blunt bodies at small angles of attack.

Solutions at zero angle of attack are obtained as a special case of the general problem. Standoff distances are predicted to higher accuracy than by any other existing method.

For a shock wave that is a parabola or paraboloid of revolution at angle of incidence to a uniform free stream having infinite Mach number and $\gamma = 1.4$, the streamline that wets the body passes through the shock wave slightly above the point where it is a normal shock wave. Hence, the body is not covered by the maximum-entropy streamline in these cases. In the Newtonian limit ($M = \infty$, $\gamma = 1$), the parabolic or paraboloidal body is wetted by the maximum-entropy streamline. For a parabolic shock at infinite Mach number, $\gamma = 1.4$, the shock wave rotates more slowly than the body as angle of attack is imposed.

V. FUTURE RESEARCH

Although the analysis presented here is for general Mach number and shock shape, results have been obtained only for certain shock shapes at infinite Mach number. Work is currently in progress to program the general problem for the IBM 7090 computer.

Since the results of these calculations in the vicinity of the sonic line might serve as input data to a characteristic program for the solution of the flow field downstream of the sonic line, possible means of improving the.convergence of the method in the vicinity of the sonic line are being explored.

One such possibility involves expanding the stream functions and density in Taylor series about an arbitrary ξ = constant line in the flow. By choosing this arbitrary line close to the sonic line, one might expect more rapid convergence for values in this region at a sacrifice of convergence in the vicinity of the shock axis of symmetry.

Another possible means of improving convergence away from the shock axis of symmetry is by applying power series expansions to quantities which vary slowly as one moves away from the shock symmetry axis, thereby reducing the magnitude of the coefficients of the higher order terms with respect to those of lower order. For example, at infinite Mach number, ρ is constant behind the shock, whereas p/ρ^γ is constant on the body. If one considers expanding the product $\rho^m \rho^{1-m}$, then $m = 1$ corresponds to expanding ρ, whereas $m = \gamma/\gamma-1$ corresponds to expanding p/ρ^γ. One might consider expanding for a value of m which is the average of 1 and $\gamma/\gamma-1$. This would then correspond to a quantity which varies more slowly as one moves away from the shock axis of symmetry than either p/ρ^γ on the shock or ρ on the body.

A further possible extension of the work is to render it applicable to hypersonic flow of real gases in equilibrium and perfect gases in thermal and chemical nonequilibrium.

VI. REFERENCES

1. Van Dyke, M. D., The Supersonic Blunt-Body Problem - Review and Extension, J. Aerospace Sci., 25, No.8, August, 1958, pp. 485-496.

2. Hayes, W. D., and Probstein, R. F., Hypersonic Flow Theory, Academic Press, New York, 1959.

3. Van Dyke, M. D., and Gordon, H. D., Supersonic Flow Past a Family of Blunt Axisymmetric Bodies, NASA TR R-1, 1959.

4. Belotserkovskii, O. M., On the Calculation of Flow Past Axisymmetric Bodies with Detached Shock Waves Using an Electronic Computing Machine, Prikl. Mat. Mekh., 24, No. 1, 1960, pp. 511-517.

5. Mangler, K. W., The Calculation of the Flow Field Between a Blunt Body and the Bow Wave, Hypersonic Flow, Butterworths Scientific Publications, London, 1960, pp. 219-239.

6. Vaglio-Laurin, R., and Ferri, A., Theoretical Investigation of the Flow Field About Blunt-Nosed Bodies in Supersonic Flight, J. Aerospace Sci., 25, No.12, December, 1958, pp. 761-770.

7. Vaglio-Laurin, R., On the PLK Method and the Supersonic Blunt Body Problem, IAS Preprint No. 61-22, January, 1961.

8. Ames Research Staff, Equations, Tables, and Charts for Compressible Flow, NACA Rep. 1135, 1953.

9. Clebsch, A., Ueber Eine Allgemeine Transformation der Hydrodynamischen Gleichungen, Crelle, 54, 1857, p. 303.

10. Gill, S., A Process for the Step-by-Step Integration of Differential Equations in an Automatic Digital Computing Machine, Proceedings of the Cambridge Philosophical Society, 47, Part 1, January, 1951, pp. 96-108.

11. Fuller, F. B., Numerical Solutions for Supersonic Flow of an Ideal Gas Around Blunt Two-Dimensional Bodies, NASA TN D-791, July, 1961.

12. Garabedian, P. R., Numerical Construction of Detached Shock Waves, J. Math. and Phys., 36, No. 3, pp. 192-205.

13. Shanks, D., Nonlinear Transformations of Divergent and Slowly Convergent Sequences, J. Math. and Phys., XXXIV, No. 1, April, 1955.
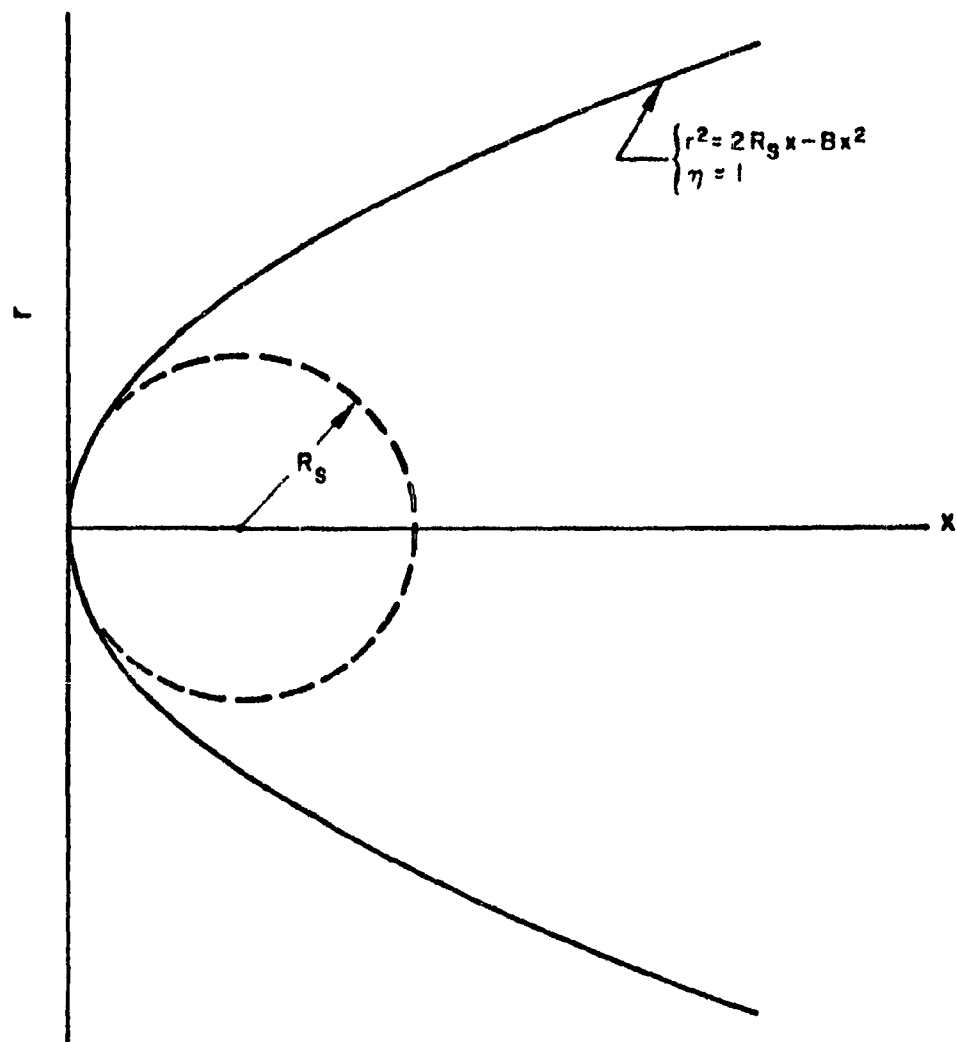
The figure shows a parabolic curve with the equation labeled:

$$\begin{cases} r^2 = 2R_S x - Bx^2 \\ \eta = 1 \end{cases}$$

with axes labeled r (vertical) and x (horizontal), and a dashed circle of radius R_S.
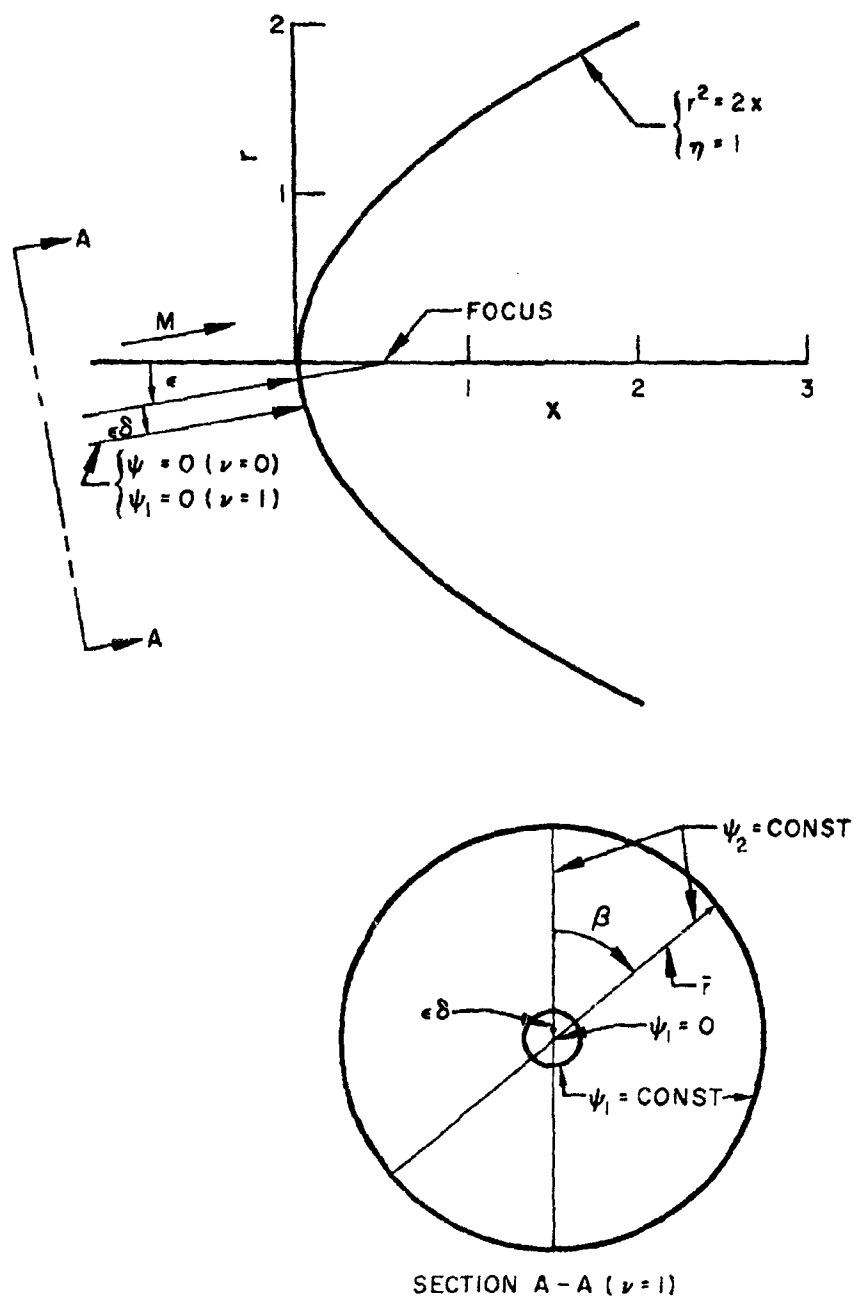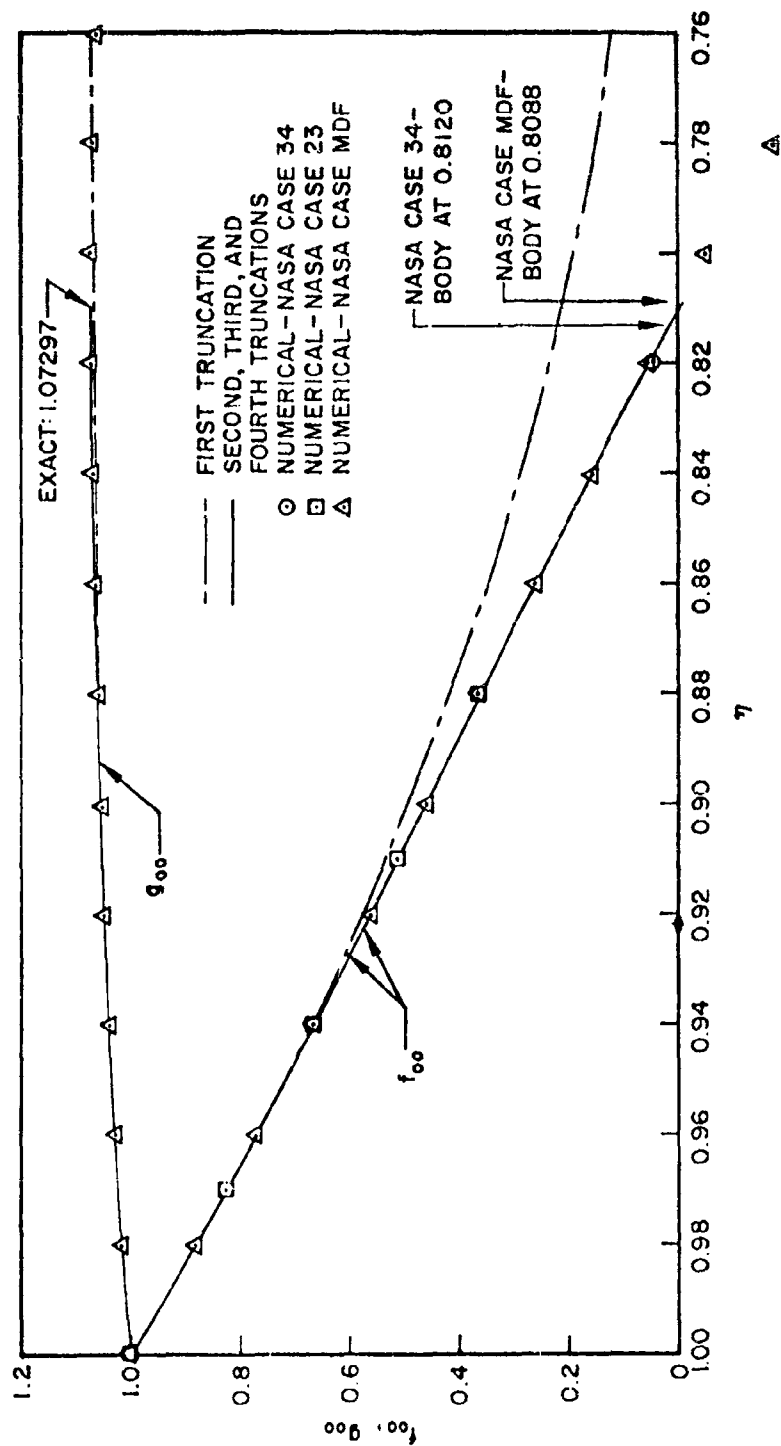
Fig. 1 Representation of Shock Wave

40

Fig. 2 Parabolic or Paraboloidal Shock Wave at Angle of Attack

Fig. 3 Variation of Reduced Stream Function ψ/ξ and Density Along the Axis
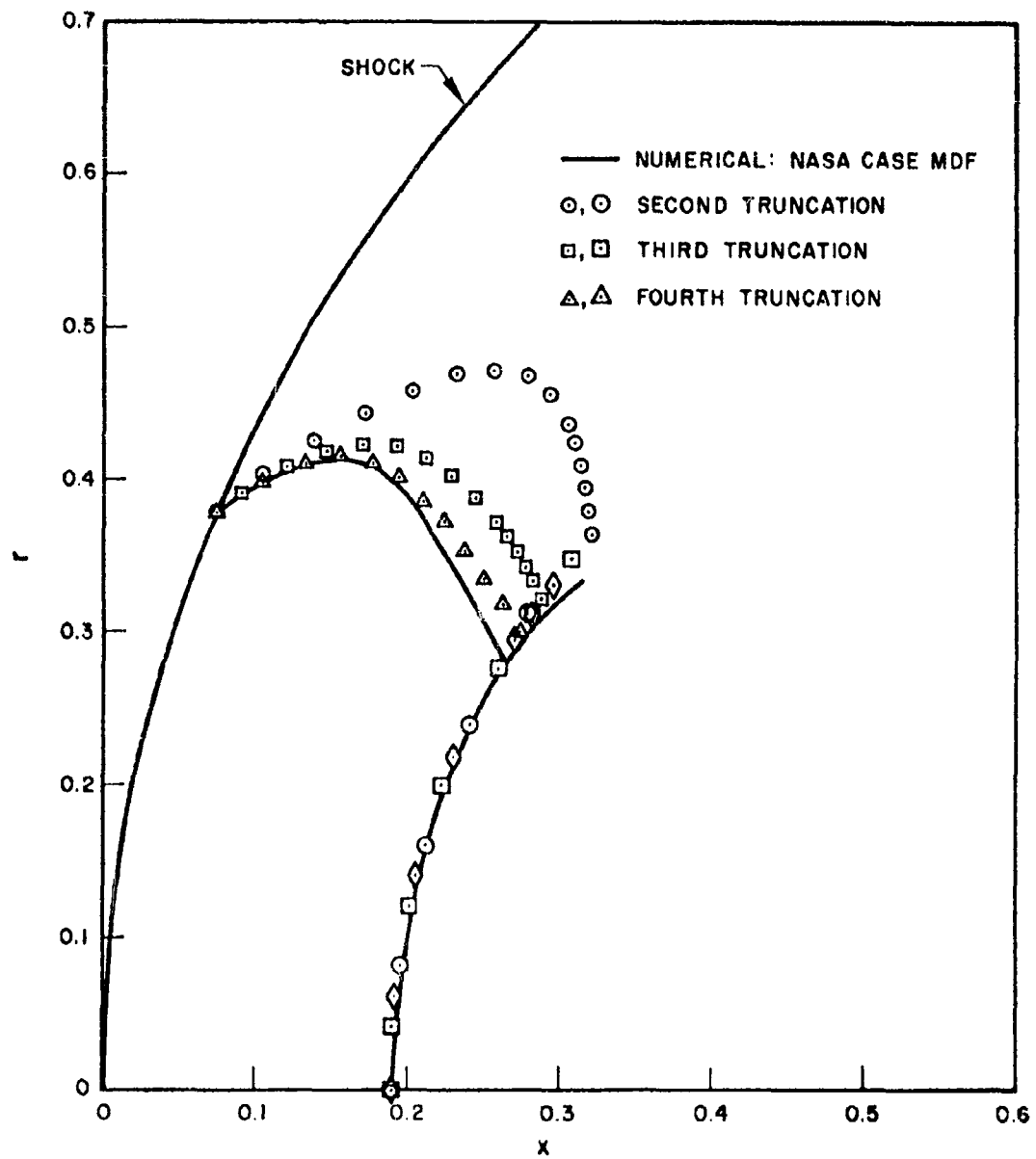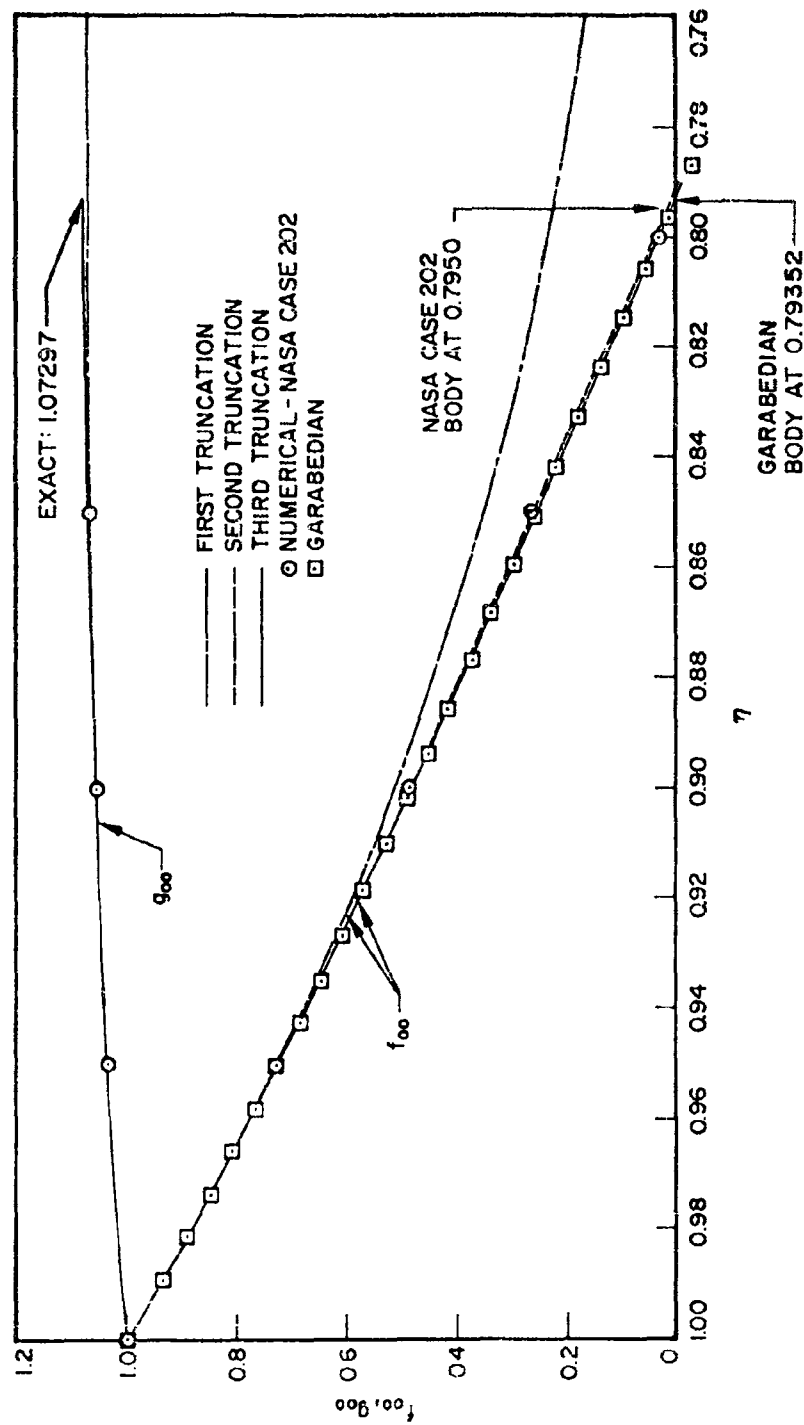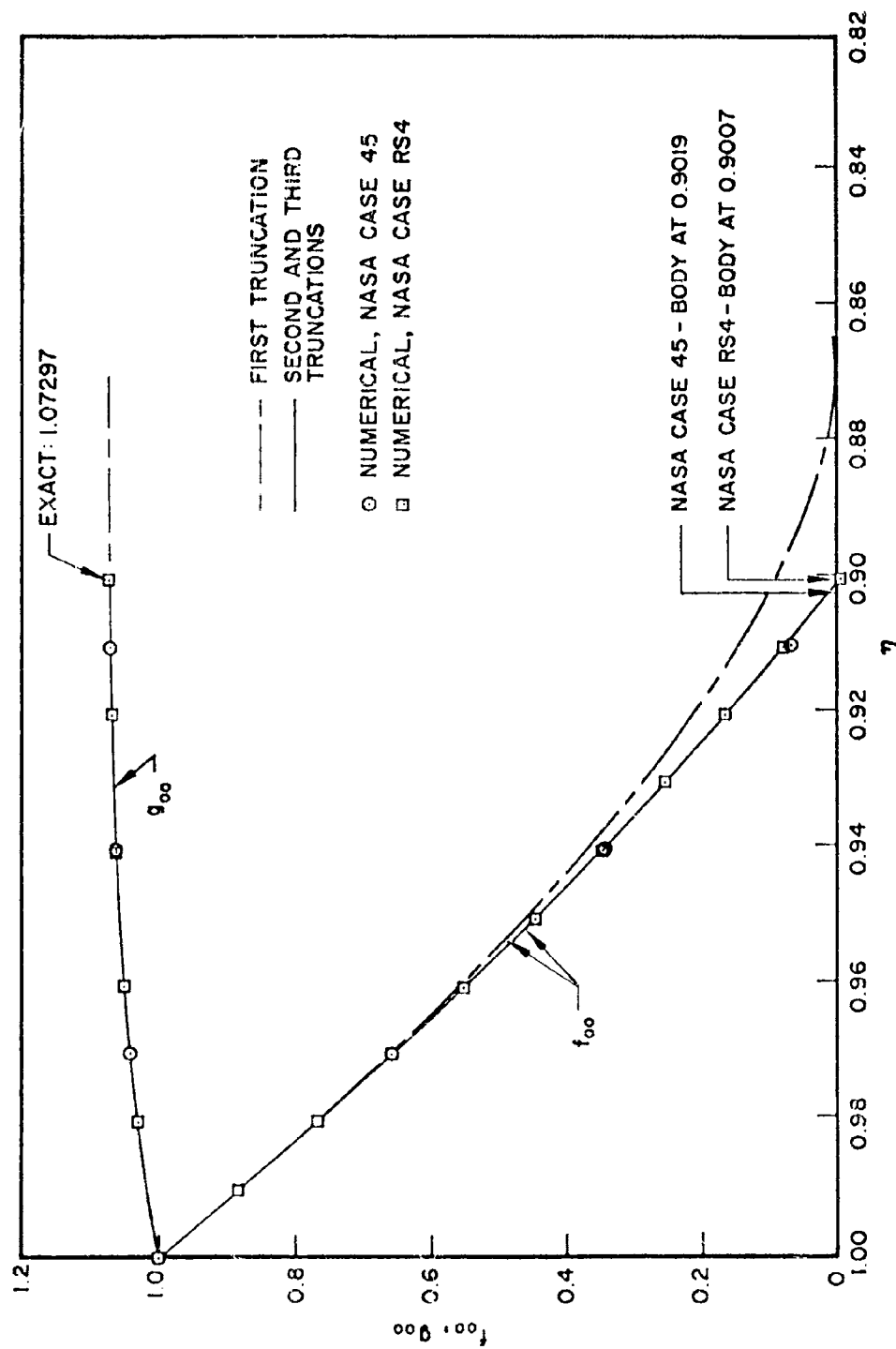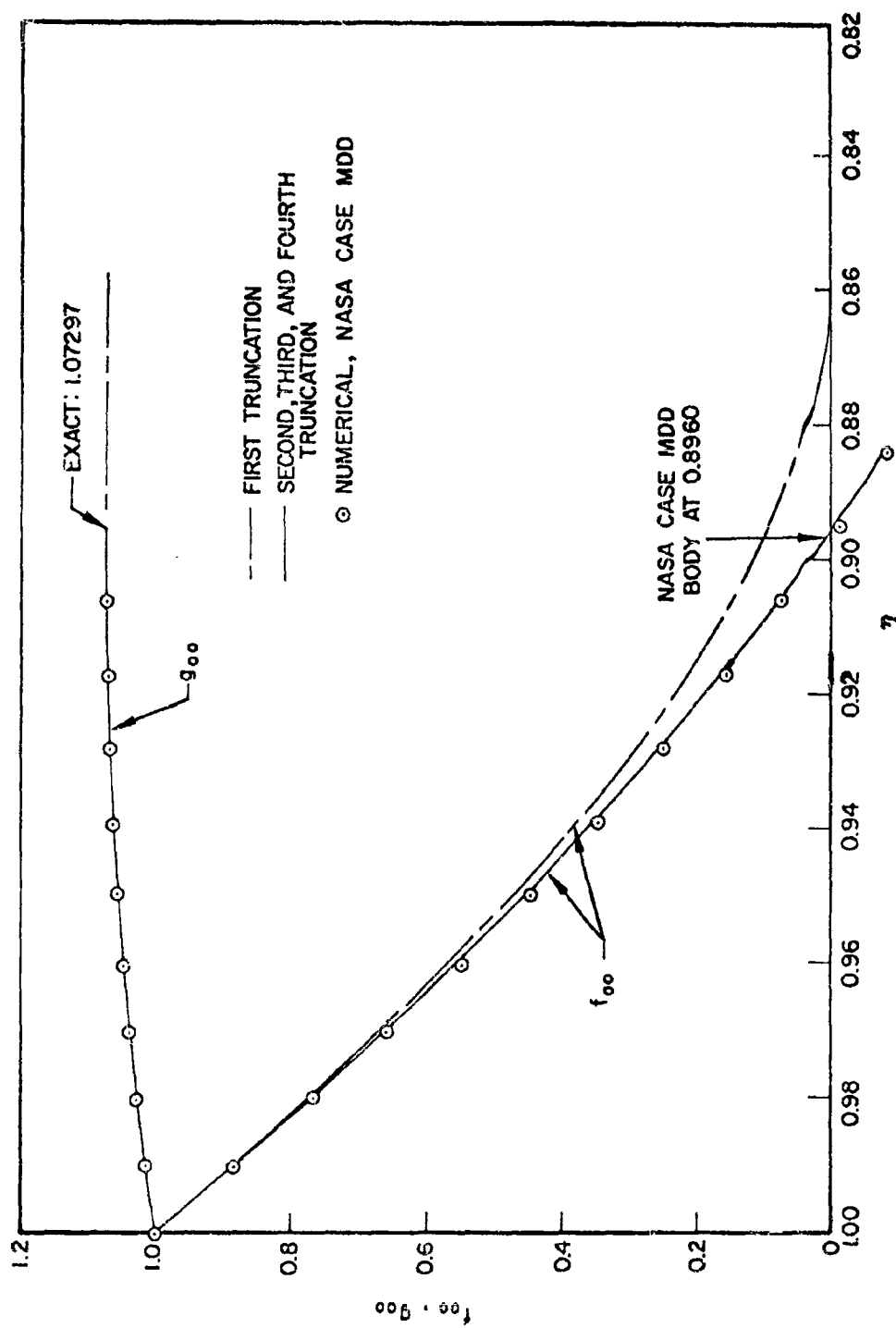Circular Shock, $M = \infty$, $\gamma = 1.4$

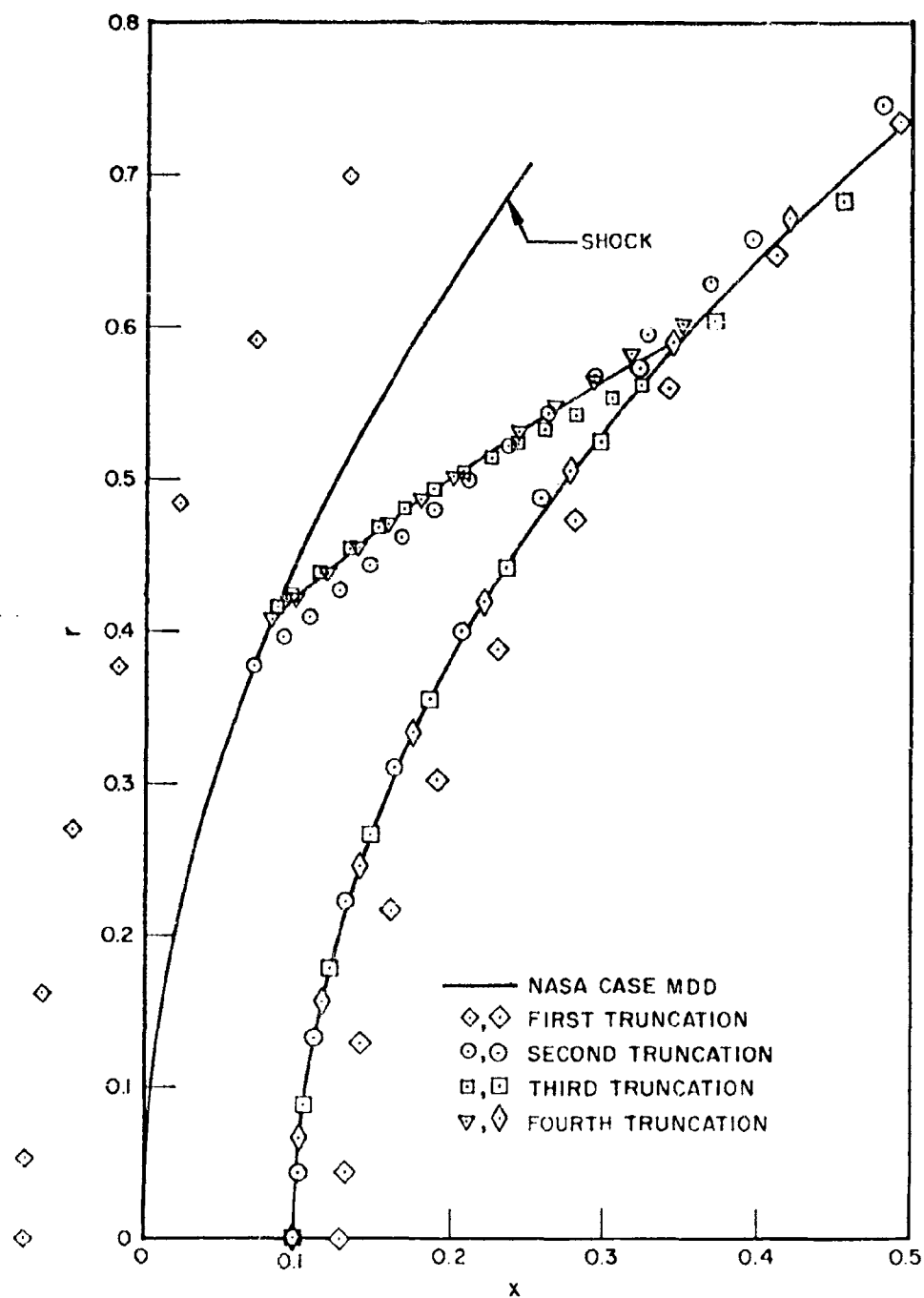Fig. 4 Comparison of Body Shapes and Sonic Lines
Circular Shock, M = ∞, γ = 1.4

43
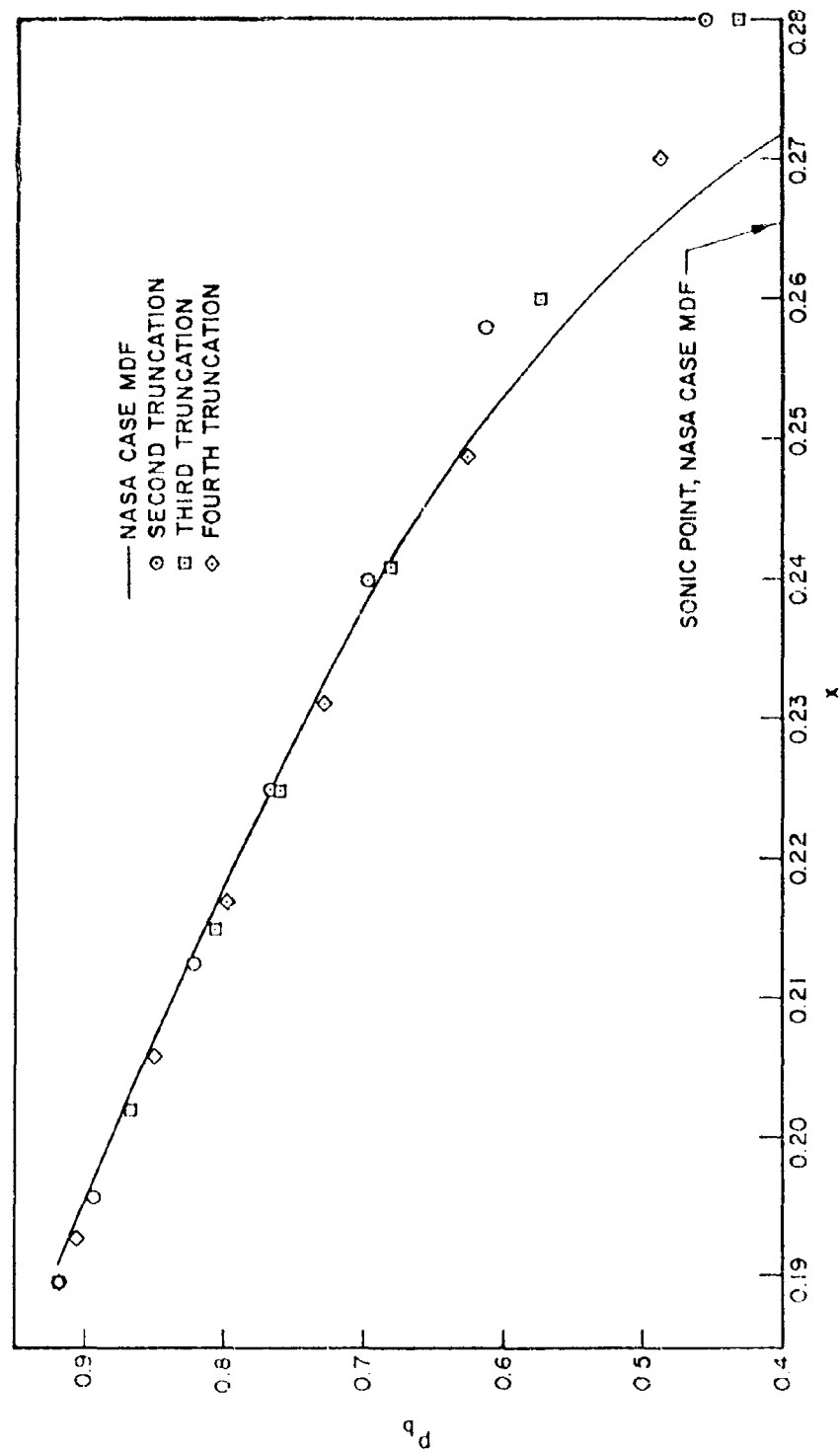
Fig. 5 Surface Pressure Distribution – Circular Shock, $M = \infty$, $\gamma = 1.4$

44

Fig. 6 Variation of Reduced Stream Function ψ/ξ and Density Along the Axis
Parabolic Shock, $M = \infty$, $\gamma = 1.4$

45

Fig. 7 Variation of Reduced Stream Function $2\bar{\psi}/\xi^2$ and Density Along the Axis
Spherical Shock, $M = \infty$, $\gamma = 1.4$

Fig. 8 Variation of Reduced Stream Function $2\psi/\xi^2$ and Density Along the Axis Paraboloidal Shock, $M = \infty$, $\gamma = 1.4$

Fig. 9 Comparison of Body Shapes and Sonic Lines
Paraboloidal Shock , $M = \infty$, $\gamma = 1.4$

48
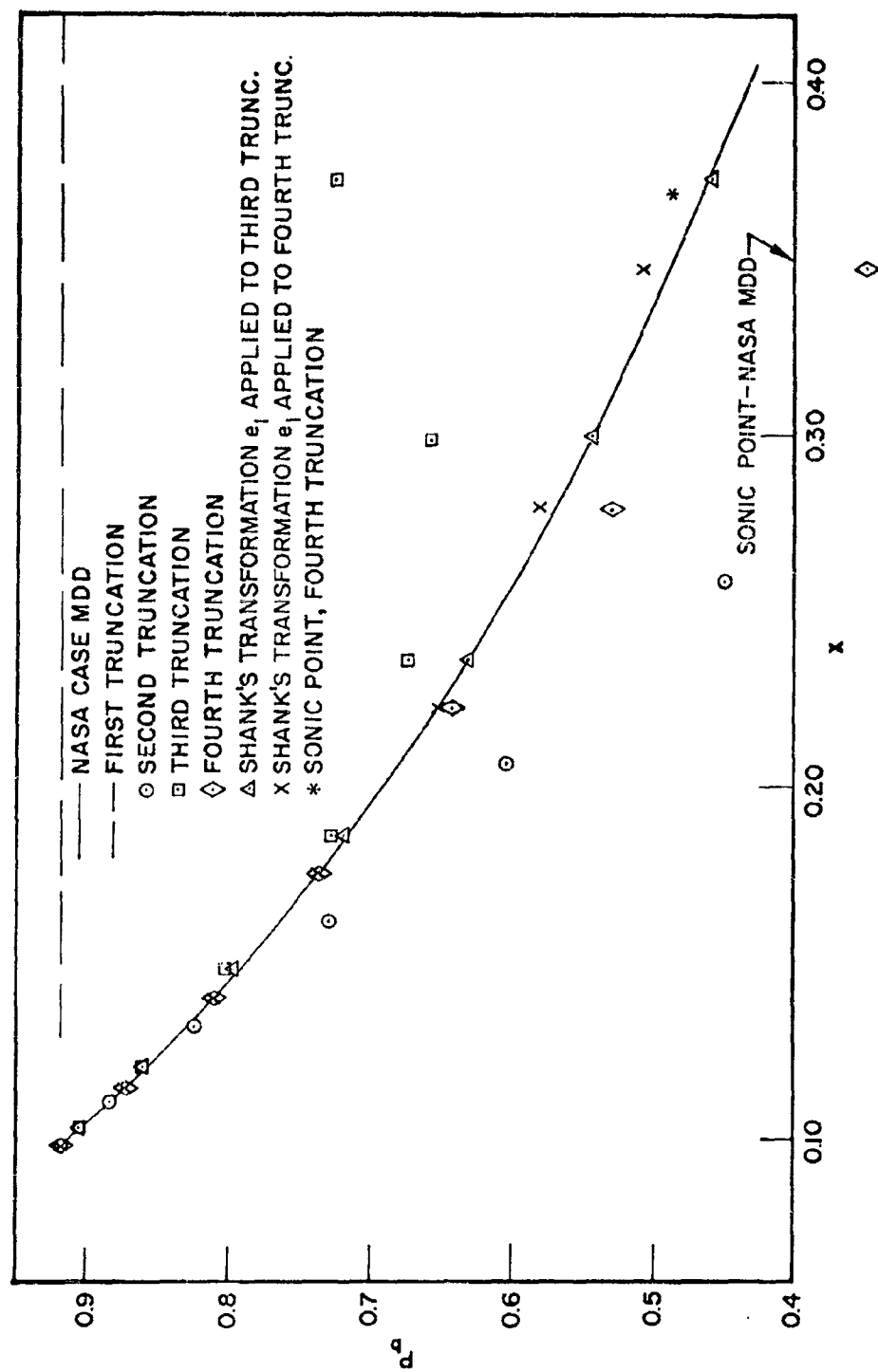
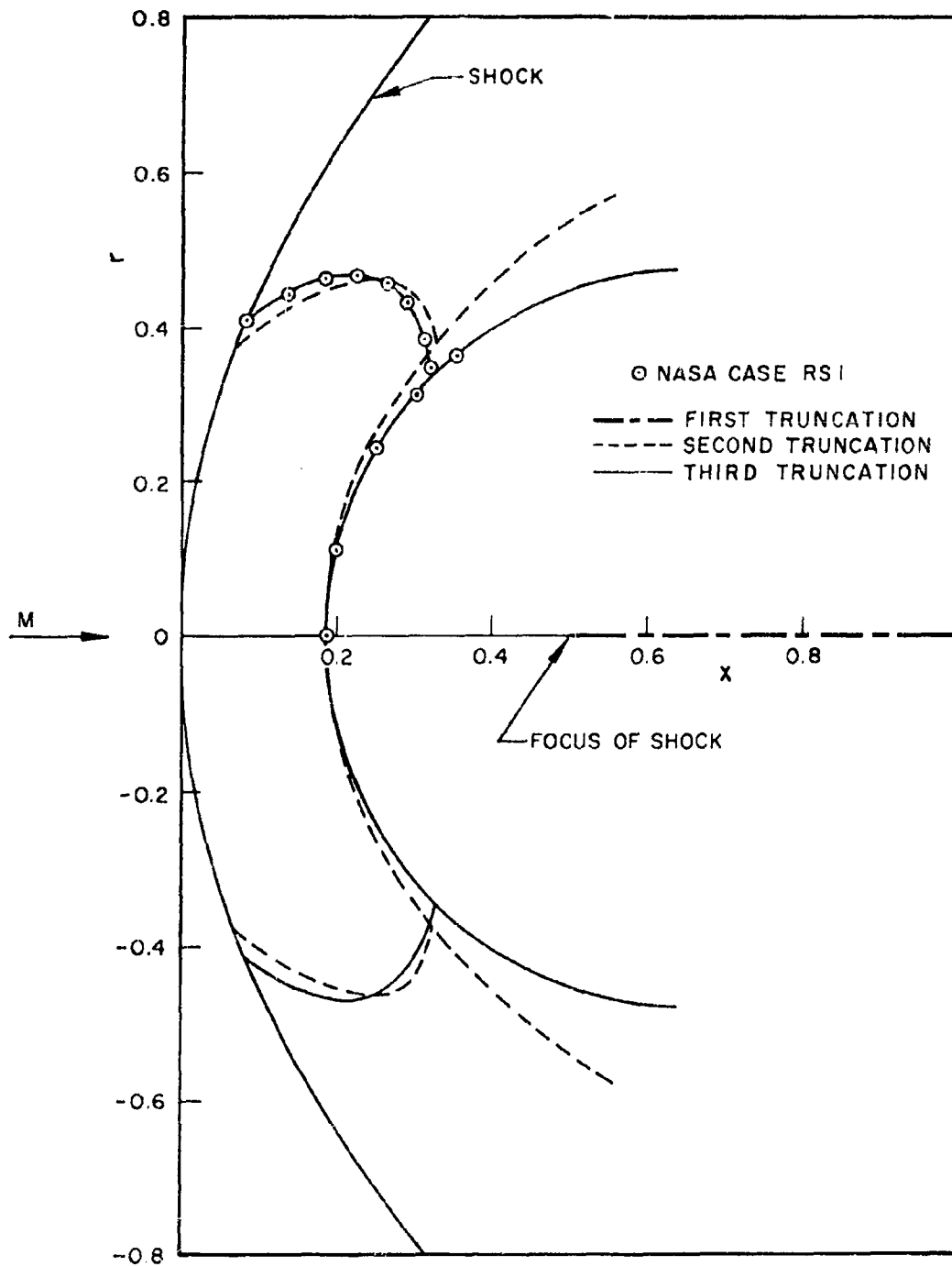Fig. 10 Surface Pressure Distribution – Paraboloidal Shock, $M = \infty$, $\gamma = 1.4$

49

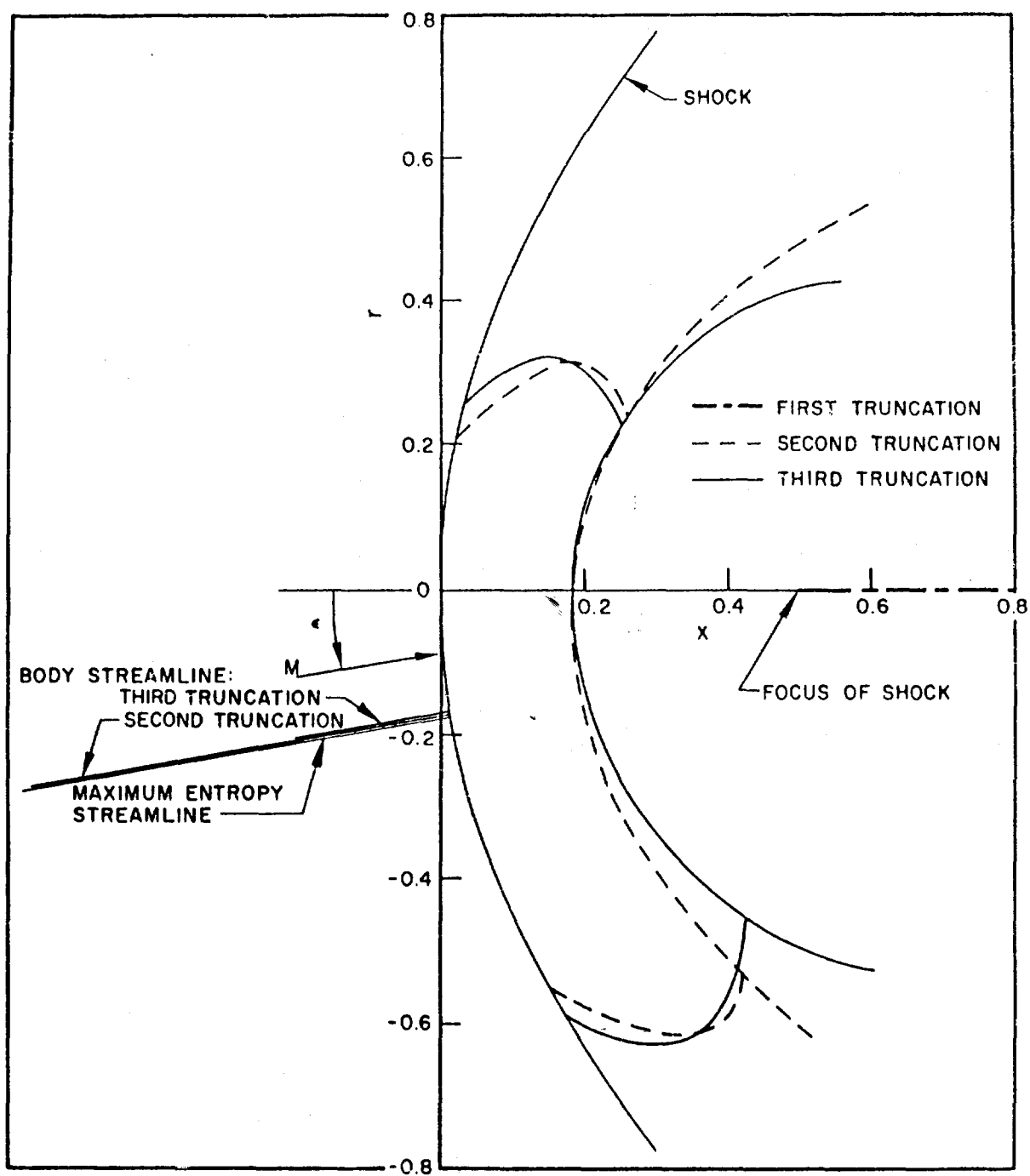Fig. 11 Body Shapes and Sonic Lines — Parabolic Shock, $M = \infty$, $\gamma = 1.4$, $\epsilon = 0°$

50

Fig. 12 Body Shapes, Sonic Lines, and Comparison of Body Streamlines With Maximum Entropy Streamline — Parabolic Shock, $M = \infty$, $\gamma = 1.4$, $\epsilon = 10°$
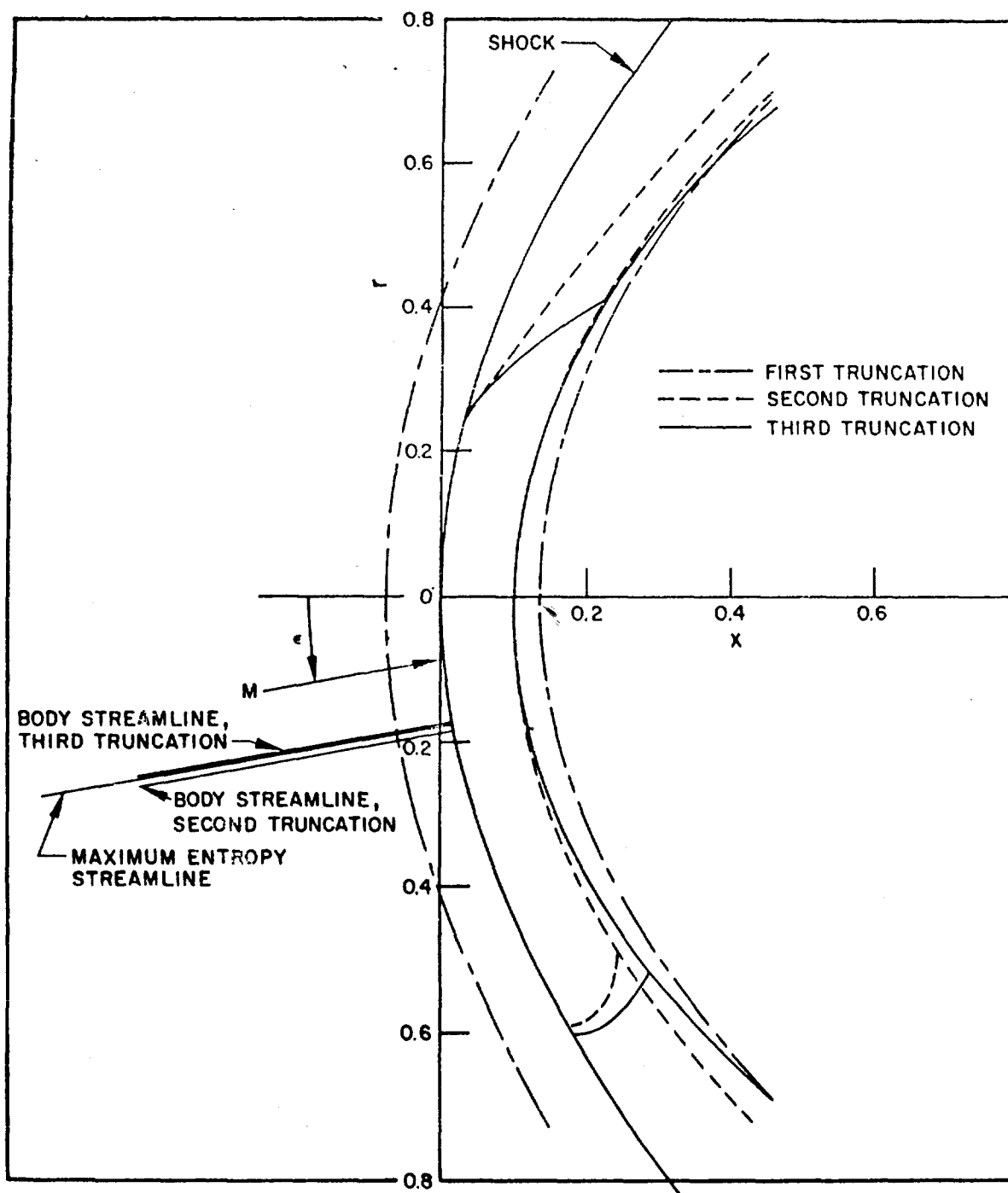
51

Fig. 13 Body Shapes, Sonic Lines, and Comparison of Body Streamlines With Maximum Entropy Streamline — Paraboloidal Shock, $M = \infty$, $\gamma = 1.4$, $\epsilon = 10°$
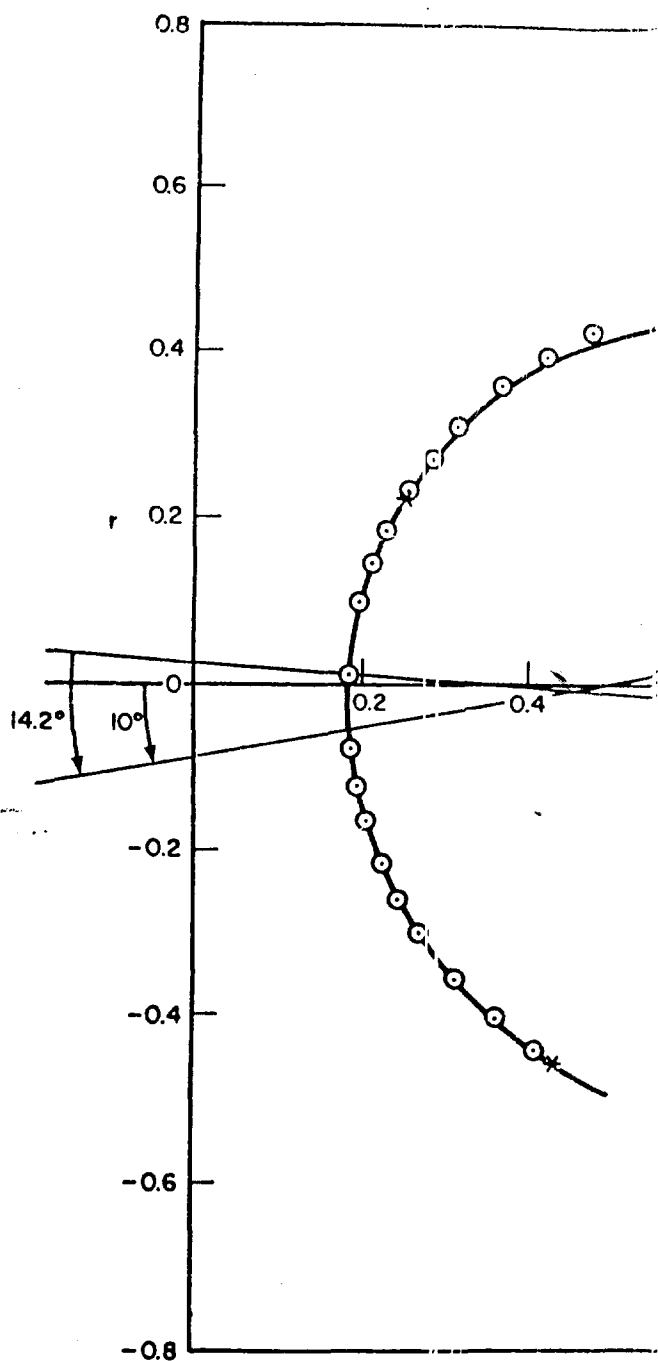
Fig. 14 Fitting an Ellipse to the Third Truncati?
$M = \infty$, $\gamma = 1$.

53